

Effects of a passive tuned mass damper on blade root impacts during the offshore mating process

Amrit Shankar Verma ^{a,b,c,*}, Zhiyu Jiang ^d, Zhen Gao ^{a,b}, Nils Petter Vedvik ^e

^a Department of Marine Technology, Norwegian University of Science and Technology (NTNU), N-7491, Norway

^b Centre for Marine Operations in Virtual Environments (SFI MOVE), NTNU, Norway

^c Department of Aerospace Structures and Materials, Faculty of Aerospace Engineering, Delft University of Technology, Kluyverweg 3, 2629HS, Delft, the Netherlands

^d Department of Engineering Sciences, University of Adger, 4879, Grimstad, Norway

^e Department of Mechanical and Industrial Engineering, Norwegian University of Science and Technology, Norway



ARTICLE INFO

Keywords:

Wind turbine blade
Mating operation
Tuned mass damper
Limiting sea states
Finite element analysis
Monopile

ABSTRACT

Single-blade installation is a conventional method for installing blades on monopile-type offshore wind turbines. A jack-up crane vessel is commonly used, and individual blades are lifted to the tower top height and mated with the hub. The relative motions between the hub and blade root during the mating phase, partly due to wind-induced blade motion and partly due to wave-induced monopile motion, can induce substantial impact forces at the blade root. This can cause severe damage at the blade root connections and have a high potential to jeopardise the installation task. Mitigation measures are therefore required to limit the relative motion between the hub and the root during the mating process. In this article, we investigate the effects of a passive tuned mass damper (TMD) on the (1) impact velocities manifested between the blade root and hub during the mating phase and (2) its effect on the response-based limiting sea states. Time-domain multi-body simulations of an installation system characterising the mating operation with and without a TMD for collinear and misaligned wind and wave conditions have been performed, and the effectiveness of TMD for controlling the impact velocity is quantified. Furthermore, finite element analyses are performed to determine the threshold velocity of impact for a scenario in which a blade root with a guide pin suffers a sideways impact with the hub. It is found that the tuned mass damper can reduce the relative impact velocities by more than 40% and can substantially expand the allowable sea states and operability for the mating operation. Moreover, the effectiveness of TMD at reducing the impact velocity increases with increasing significant wave height (H_s); however, it decreases with increasing wind-wave misalignment and with shifts in the wave spectral peak period (T_p) away from the tuned frequency. The findings of the study can be utilised for planning safe and cost-efficient installation of latest-generation wind turbine blades.

* Corresponding author. Department of Marine Technology, Norwegian University of Science and Technology (NTNU), N-7491, Norway.

E-mail addresses: a.s.verma@tudelft.nl (A.S. Verma), zhiyu.jiang@uia.no (Z. Jiang), zhen.gao@ntnu.no (Z. Gao), nils.p.vedvik@ntnu.no (N.P. Vedvik).

1. Introduction

1.1. Background

The growing demand for renewable sources of energy in recent times has led to the rapid development of the offshore wind turbine sector [1]. Among different offshore wind turbine concepts, monopile-type offshore wind turbines currently dominate the market and account for more than 87% of the total turbines installed in European waters [2]. The installation methods for these turbines usually involve a split-type procedure in which components are transported in unassembled pieces and are installed at the site piece-by-piece [3]. At the offshore site of installation, first, the upended monopile is hammered into the sea bed, and the transition piece is mated with the hub. Then, the components of the turbine – i.e., the tower, nacelle, hub and rotor blades – are separately lifted and assembled in sequence.

In the single-blade lifting process (Fig. 1(a)), a jack-up crane vessel is usually involved [4], as these vessels have legs that are anchored into the sea bed and thus provide a stable platform during the lifting phase [5]. The blade lifting process includes the attachment of yoke to the blade mass centre, lifting the blade and yoke system to the hub height by a crane, and finally mating the blade root with the hub of the turbine [6]. The mating phase of the blade, in which several bolted connections of the blade root are mated with the pre-assembled hub (Fig. 1(b)), is a challenging task [7]. The difficulty is due to excessive relative motions between the root and the pre-assembled hub, which can cause impact loads at the blade root and thus damage the root connections. This has a high potential to negatively affect the blade's structural integrity, given that the root of a blade experiences its maximum bending during the operational phases [8,9].

The relative motions during the mating phase are governed by the individual responses of the pre-assembled hub and lifted blade. Hub motions are caused by wave-induced loads on the monopile structure, whereas blade root motions are caused by wind-induced loads on the lifted blade. A monopile is typically a cantilever structure, of which one end is anchored into the seabed and is extremely sensitive to wave-induced loads [10]. One of the concerns is its limited structural, aerodynamic and hydrodynamic damping characteristics; the overall damping ratio of monopile in its first fore-aft mode is approximately 1% [11,12]. The damping attribute is even more critical during installation phases, as aerodynamic damping from the blades is absent [6]. Consequently, the mating process in wave conditions with a spectral peak period close to the eigenfrequency of the monopile causes significant resonance-driven tower top motions in the hub, especially contributed from first structural modes of vibrations - i. e, first fore-aft bending mode and first side-side bending mode. These motions make the overall mating process vulnerable to impact loads and thus can jeopardise the entire installation task.

Currently, in the industry, blade mating procedures are planned mainly considering the blade root responses alone, and 8–12 m/s of allowable mean wind speed has been reported as a safe working limit [5,13]. Previous research has focused on improving the aerodynamic performance of wind turbine blades during the lifting process. Numerical tools by Refs. [13,14] and specialised equipment such as Boom Lock devices [15] and automated tagline systems [16] are being developed to improve the mating process; however, these exclusively consider measures for controlling the blade root responses alone. Nevertheless, based on industry interactions [17] and work by Jiang et al. [5], it has been found that the hub motions that arise due to wave-induced monopile motions are equally critical during the mating process and pose great challenges. Verma et al. [7] performed a detailed impact assessment of a blade root impacting a hub, considering the relative impact velocities during mating process, and found severe damage at the root connection, which can cause substantial delays in the installation task. Overall, dynamic motions in the hub contributed from the first mode of structural vibrations is an important parameter during the offshore mating process.

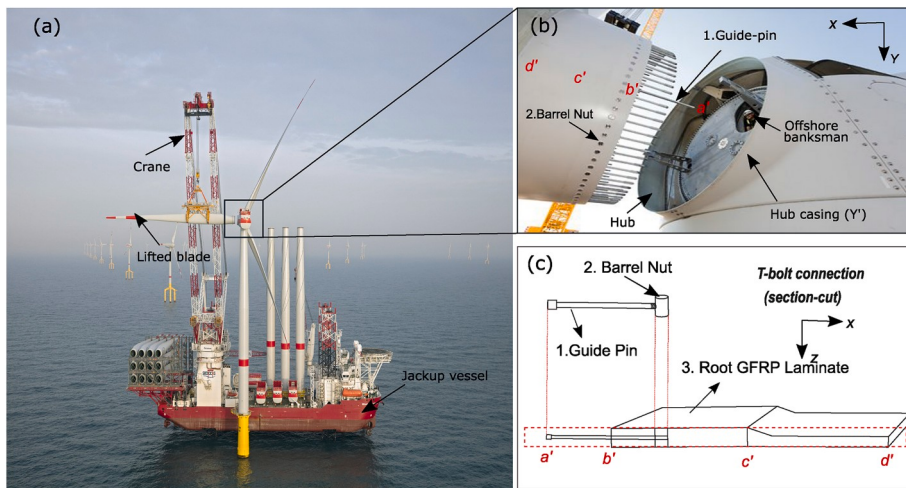


Fig. 1. (a) Lifting of blade using jack up crane vessel [18] (b) Enlarged view illustrating blade root connection while mating with hub [19] (c) A typical T-Bolt connection at the blade root (section cut a'b'c'd').

Using mitigation measures are desirable, for instance, external damping devices are used to mitigate excessive dynamic vibrations in a generic engineering structures such as bridges and tall towers. In principle, these devices can also provide effective solutions by absorbing excessive dynamic responses in the hub developed during the blade mating process. In the current paper, we investigate the application of an external damping device - a passive tuned mass damper (TMD) system - installed inside the tower structure for blade root installation phase onto the hub. However, a detailed literature review of existing vibration control techniques used in different engineering structures and especially applied to wind industry is presented below.

1.2. Types of vibration control techniques

There can be - passive, active, or semi-active type of dampers added to any mechanical system in general [20] to inhibit vibrations when subjected to external sources. Passive dampers are simple and do not require any external source of power for energy dissipation. However, it is necessary that the damping system is adjusted according to the system characteristics such that the excessive energy at the certain frequency of interest can be absorbed. Active dampers require external power sources and are complex in nature, requiring control systems to reduce the dynamic responses [21]. One of the examples of such an active damping device is a dynamic positioning system utilised in an offshore vessel. Semi-active dampers, on the other hand, combine features of passive and active dampers; their efficiency in reducing the responses of a system can equal that of an active system, but they require less power and can be operated with a battery [6,20].

Among them, passive dampers are one of the most reliable, effective and versatile damping devices and have been commonly applied in civil engineering structures to inhibit responses due to harmonic, wind and seismic loads. There exist a variety of passive damping devices in the literature, such as - tuned mass dampers (TMDs) (see Fig. 2(a)) [24–26], tuned liquid column dampers (TLCDs) (see Fig. 2(b)), and tuned liquid dampers (TLDs) (see Fig. 2(c)) [27,28]. TMDs consist of a mass, and a spring, and, can also consists of a dashpot element which represents coulomb damping. Also, as the name suggests, they reduce excessive dynamic motions of a mechanical system or a structure by the virtue of their inertial force. The frequency of a TMD is tuned to a specific natural frequency of a structure such that once the system is excited, it resonates out of phase with the motion of the primary structure to which it is attached. On the other hand, tuned liquid damper (TLD) consists of a tank partly filled with liquid, where the water depth aids in tuning the sloshing frequency of liquid with the critical frequency of the primary structure. Once the critical frequency is excited, the liquid sloshes and inhibits the excessive dynamic motion responses of the structure by exerting inertial forces onto the primary structure. Further, TLCD are special type of TLDs, and consists of liquid filled in an U-tube container, and the excessive vibrations are controlled by upward and downward motion of the water in left and right container of the U-tube while flowing through a small orifice plate. The tuning of TLCD requires a careful design of geometrical parameters that include suitable selection of cross section of U-tube container, radius of the orifice, and length of left and right U-tube columns. Note that there are also other damping devices used in the literature for generic engineering structures which include piezoelectric dampers [29,30], semi-active stiffness dampers (SASD) [31] and magnetorheological (MR) fluid dampers [32].

1.3. Vibration control techniques used in wind industry

Among several damping devices discussed above for typical engineering structures, passive TMD, because of its simplicity and high efficiency has been studied extensively and practically utilised in the wind industry. Single-TMD consists of a single degree freedom system with one large mass, and installed in the nacelle or the tower of the turbines. Such devices mainly are aimed to mitigate dynamic motions contributed explicitly from first mode of vibrations. Murtagh et al. [33] investigated the use of a STMD to mitigate the tower top vibrations induced by wind-induced loads. The studied showed high efficiency in reducing the tower top displacements, thereby showing a high merit of TMD system. Lackner et al. [21] utilised this concept and investigated use of two independent TMD system installed in the nacelle using a modified FAST code, to mitigate dynamic motions in the tower contributed from first mode of tower vibrations in both side-side and fore-aft bending mode. The case studies were presented for bottom fixed offshore wind turbine as well as for floating-type offshore wind turbine [21,34–36]. For floating type offshore wind turbines, there were applications of TMD assembled in nacelle [34,37,38] as well as in the hull [39–41]. Some other application of STMD in the published literature sources for wind turbines is tabulated in Table 1 and can also be found in a recent review paper from Ref. [42]. Nonetheless, the STMD has also been widely utilised in industrial applications. For instance, Fig. 3(a) presents a TMD developed by ESM GmbH [23], where a heavy

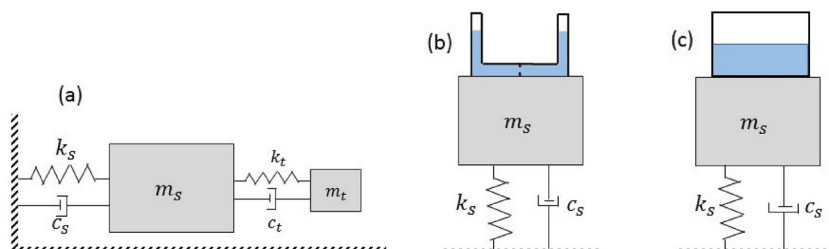


Fig. 2. Different types of passive dampers: (a) TMD (b) TLCD (c) TLD.

Table 1
Application of different passive vibration controlling techniques for WT.

Type of passive damping device	Reference
Single-Tuned Mass Damper (STMD)	[21,33,34,37–39,43,44]
Multiple-Tuned Mass Damper (MTMD)	[45–48]
Inerter-based Tuned Mass Damper system	[49,50]
Bidirectional-Tuned Mass Damper (BTMD)	[35,51–55]
Tuned liquid damper (TLD)	[56–60]
Tuned liquid column damper (TLCD)	[27,28,61–64]



Fig. 3. Tuned mass dampers used in the wind turbine industry (a) TMD mounted below the nacelle [22] [Source: ESM GMBh] (b) Artistic impression of TMD mounted in the tower of the turbine [23] [Source: Xi Engineering consultants].

mass is hanging below the nacelle. Any motion of the tower top causes the oscillation motion of the hanging mass, which is operating in an oil bath, and damps out the excessive motion. Similarly, Fig. 3(b) also presents a TMD designed by Xi Engineering consultants [22], called SQT (Seismically Quiet Tower), and is mounted in the tower of the turbine. This has been used in the sites where in the vicinity, there are sensitive seismic devices, and any tower top-induced vibrations are required to be inhibited in getting transferred to the ground.

Further, there has also been use of multiple-TMD devices that consists of several TMDs with different masses, which are considerably smaller than one single mass of STMD. These are installed in the wind turbine to reduce vibrations in both first and second modes of vibrations, especially for applications where there is high vulnerability of wind turbines against seismic excitation and largest displacement might not occur at the tower top. For instance, Zuo et al. [45] investigate the application of MTMD where three different arrangement configurations of tuned mass dampers were used to mitigate dynamic motions against first and second mode of vibrations. The results from their study showed that the external devices aided not only in counteracting first mode of vibrations but also higher mode of vibrations. Moreover, the MTMD was found more efficient than STMD for structures susceptible to motions from multiple modes of vibrations. Hussan et al. [46] also used MTMDs, where one set of TMD was installed at the top and other configuration was installed at the bottom base of the tower, and seismic excitations were considered. Again, the results showed MTMD being more efficient in suppressing excessive dynamic motions from several vibration modes, where as MTMD being more advantageous for dynamic motions from single mode of vibrations. In recent years, there are also have been application of inerter-based vibration control systems [49,50] that have been investigated for reducing the dynamic responses of the wind turbines. This system reduces the physical mass of a generic TMD substantially, and helps in achieving similar performance as compared to traditional TMD but with reduced mass and less stroke of TMD. Such a system proves efficient in their arrangements in the nacelle of a turbine which has space restrictions.

Since the dynamic motion responses in the hub are critical during the blade root mating phase and are mainly contributed from the first structural mode of vibrations, STMD is considered in this study, and will be referred to as passive TMD in the rest of the paper. Note that there are other sophisticated configurations of external passive damping devices such as bidirectional TMD, TLD, and TLCD, used in the literature applied to different wind turbines. Their detailed review is out of the scope of the paper, however, can be found in Ref. [42] and is also summarised in Table 1.

1.4. Novelty and objective of the paper

The application of different external damping devices presented above were focused on controlling responses of wind turbines during the operational and parked conditions of wind turbines. However, there are very rare studies performed in the literature for installation phases. As discussed earlier, the hub motions are critical owing to absence of aerodynamic damping of the blades - thereby making installation phase including lifting and mating of nacelle and blades with hub challenging. Jiang et al. [65] investigated the effects of single tuned mass damper on installation of wind turbine nacelle onto the hub. A 10 MW turbine was considered and it was

found that the short term extreme responses were reduced by more than 50% in the sea states with period ranging between 4 and 12 s. Also, for the blade installation phase, Jiang et al. [6] considered the application of TMDs for the single-blade lifting process; the results demonstrated effective damping of hub motions. However, the results were focused on collinear wind-wave conditions alone, and the effects on critical parameters such as impact velocities and damage to the blade root were not considered. These parameters must be quantified to derive response-based limiting sea states, which is critical for the safety of the mating task. In this work, we investigate the application of a passive tuned mass damper (TMD) system, installed inside the tower structure during the installation, on (1) the impact velocities manifested between the blade root and hub during the mating phase and (2) the response-based limiting sea states. In addition, we also consider the effect of wind-wave misalignment on the efficiency of TMDs given that such environmental conditions exist during the mating process. Overall, the novelty of the paper is to combine theory with practice and present the merit of TMDs during the blade installation phase, together with parameters that determine safety of the blade root mating operations. Further, the results of the paper is expected to provide recommendations and guidelines regarding the application benefit of TMD systems to the safety of installation tasks.

The remainder of the paper proceeds as follows. Section 2 presents the problem definition, including the overall analysis procedure followed in this work. Section 3 presents the material and modelling method. Section 4 presents and discusses the results, emphasising the effect of the tuned mass damper on the wind turbine blade mating procedure. Finally, section 5 concludes the paper.

2. Problem definition

2.1. Critical scenario

A wind turbine blade has embedded mechanical joints and bolted connections at its root, which enables its attachment to the hub of a turbine [66,67]. Commonly, a T-bolt type connection is used, which is uniformly spread throughout the circumferential area of the blade root. Each T-bolt connection consists of a steel barrel nut and a steel bolt and is drilled into the root laminate made of GFRP material [68] (Fig. 1(c)). During the mating process, a few longer bolts called guide pins are present at the blade root (see Fig. 1(b)-(c)), and they aid the offshore banks-man present in the hub to visually monitor the alignment process [7]. The guide pins are the first bolts to enter the hub of a turbine and thus are exposed to higher impact risks than other normal-sized bolts. Once, the wind turbine blade is successfully mated with the hub, the guide pins are then replaced with normal-size bolts.

During the mating process, there are two most likely impact scenarios that can occur when the guide pin is being mated with the hub. These are head-on impacts and sideways impacts between the guide pin and hub [7] (Fig. 4). The head-on impact scenario occurs when the relative motion between hub and blade root is predominantly in the x-direction (see Fig. 4), whereas sideways impacts occur due to relative motion between hub and blade root in the y-direction. It was already discussed in Refs. [7] that a head-on impact is not as likely to be critical compared to the sideways impact since the bolt suffers the impact in its axial direction, which is designed to endure maximum loads during operation. On the other hand, sideways impacts induce transverse impact loads on the bolt, causing severe bending of the guide pin and further damage to the root laminate. It was found in Ref. [7] that damage developed at the blade root in the sideways impact scenario causes the lifted blade to be brought back to the vessel, requiring repair, and thus could delay the installation task. In this paper, we consider sideways impacts as critical and investigate the effect of a tuned mass damper on the relative impact velocity between hub and blade root in the global y-direction. Note that the global y-direction corresponds to an earth-fixed global coordinate system xyz used in the numerical modelling of the installation system in HAWC2 and represents motion of the hub in the fore-aft direction. The modelling procedure will be explained in detail in section 3.

2.2. Analysis procedure

Fig. 5 outlines the analysis procedure followed in this study for investigating the effect of a passive tuned mass damper on the wind turbine blade mating procedure. The procedure is divided into two independent but related steps. The first step is an analysis of the installation system based on multibody simulations. Here, the preassembled monopile system and lifted blade system with different

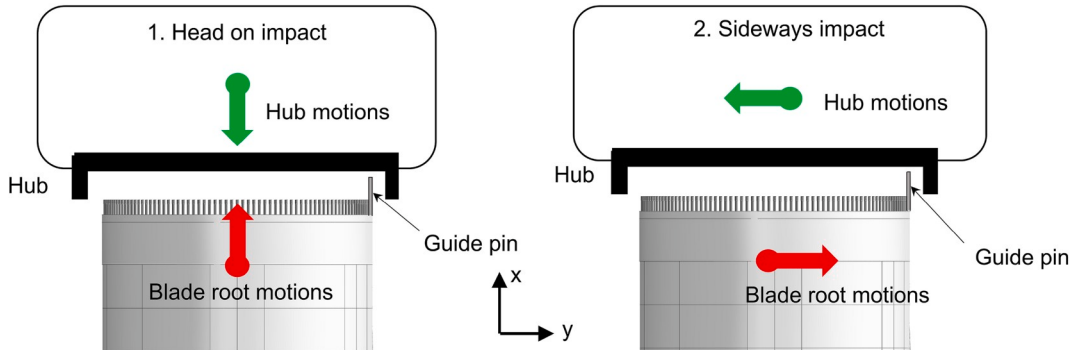


Fig. 4. Impact scenario between guide-pin and hub.

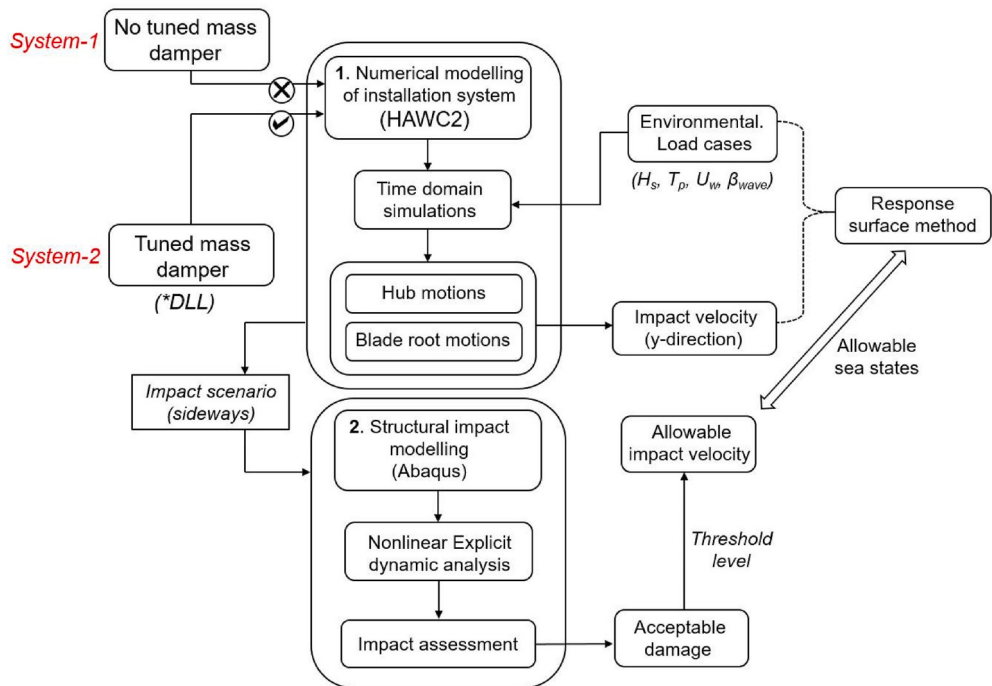


Fig. 5. Numerical analysis procedure.

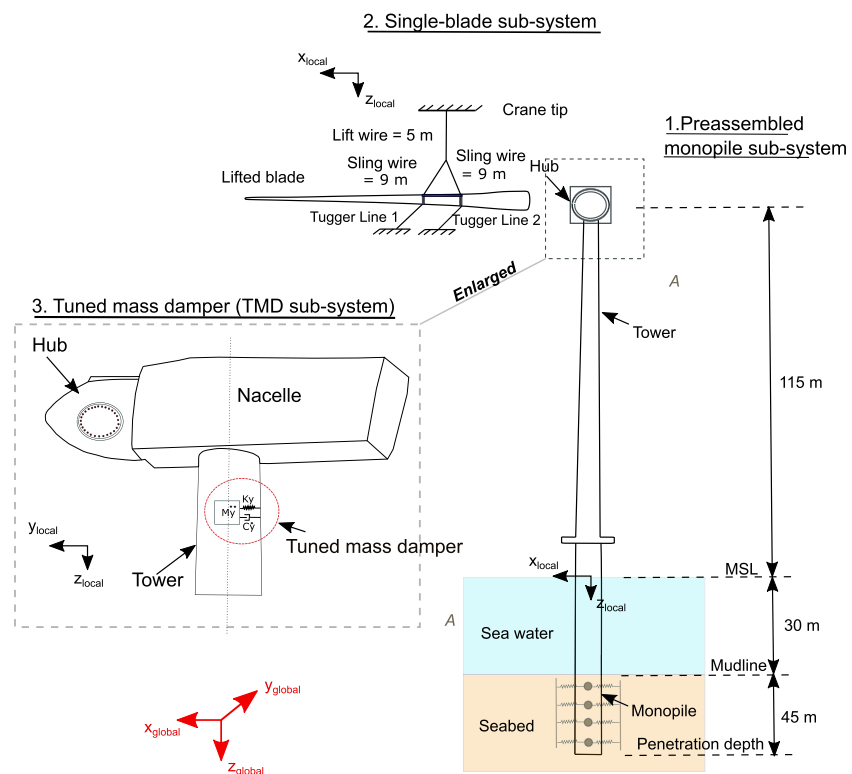


Fig. 6. Details of different sub-systems modelled in HAWC2 for characterising mating operation.

components involved during the wind turbine blade mating procedure are numerically modelled using the HAWC2 code [69]. Time domain simulations are performed for two different installation system, i.e., with and without a passive tuned mass damper installed inside the tower wall structure. Different load cases expressed in terms of sea state parameters – i.e., significant wave height (H_s), wave spectral peak period (T_p), mean wind speed (U_w) and wind-wave misalignment angle (β_{wave}) – are considered. The blade root motions and hub motions are analysed, and the impact velocity in the y-direction, which is found to be critical for the blade root impact in the sideways direction, is quantified. Then, the impact velocities obtained for different load cases are related to sea state parameters based on the response surface methodology, and the response surfaces are compared between installation systems with and without a TMD.

The next step in the analysis procedure is a finite element analysis of a case in which a single guide pin at the blade root impacts the hub in the sideways direction. A detailed three-dimensional finite element model for the T-bolt connection consisting of a barrel nut, guide pin bolt, and root laminate is developed based on a previous study [7]. Nonlinear dynamic explicit analyses are performed for different impact velocities, and the threshold level for the impact velocity is estimated. The details of the failure index and material models will be described in section 3. Finally, the allowable impact velocity estimated from finite element analysis is mapped with response surfaces obtained for impact velocities, and the effect of the TMD on the limiting sea states for the mating task is quantified.

3. Modelling method

3.1. Numerical modelling of the installation system

The installation system describing the mating phase was numerically modelled in HAWC2 [70], which is an aeroelastic code based on multi-body dynamics. The code is developed by the Technical University of Denmark and is capable of performing time domain response simulations of wind turbines under the action of external applied loads. The HAWC2 code also consists of advanced features such as the capability to include any external effects on the wind turbines through a DLL (dynamic link library). In this paper, we consider a passive tuned mass damper inside the tower structure of wind turbine (Fig. 6) through a DLL feature written in Fortran, which is linked with HAWC2 main program.

The wind turbine blade mating process modelled in HAWC2 consists of three sub-systems (Fig. 6). These are (1) a preassembled monopile sub-system consisting of a monopile anchored into the sea bed and an assembled system of tower, nacelle and hub mounted on the monopile; (2) a single blade-lift sub-system consisting of the lifted blade, lift wires and tugger lines; and finally, (3) a tuned mass damper device that is placed inside the tower structure. Note that in this study, the jack-up crane vessel is not explicitly modelled, and the crane tip is generalised with a fixed boundary condition. Nevertheless, since the vessel legs are anchored into the seabed and provide a stable crane tip position during mating, the fixed-crane-tip idealisation of the vessel is an acceptable assumption. The models of the individual sub-systems are discussed below.

3.1.1. Assembled monopile sub-system

The assembled monopile sub-system modelled in HAWC2 consists of a monopile structure, tower, nacelle and hub, as shown in Fig. 6. The DTU 10 MW wind turbine [71] is considered as the base model in this study, and thus all the parameters except those of the monopile structure are based on the reference turbine. The design parameters for the monopile support structure are derived from Refs. [72]. The pile has a diameter of 9 m and is anchored into the seabed, consisting of uniform sand layers with a penetration depth of 45 m below the mudline. The $p - y$ curve for describing the lateral stiffness of the soil is also derived from Ref. [72]. The monopile structure is modelled with Timoshenko beam elements, whereas the soil is described by a distributed spring model. This modelling approach regards the pile as a flexible foundation with a free-free beam condition, with lateral springs distributed through the adjoining soil portions [5]. The damping ratios of the original monopile in the first-aft and side-side modes are calibrated to 1% and are based on the experimentally obtained values from Ref. [11,73]. The attributes of different components of the monopile sub-system are summarised in Table 2.

The monopile structure is exposed to wave-induced hydrodynamic loads. These loads are estimated in HAWC2 using the Morison

Table 2
Characteristics of different components of installation system modelled in HAWC2.

Parameter	Symbol	Value
Diameter of monopile (m)	D_m	9
Monopile penetration depth (m)	P_m	45
Water depth (m)	d_w	30
Natural period of first-fore aft mode (s)	T_{FA}	4.2
Damping ratio of first-fore aft mode	ζ_{FA}	1%
Blade mass (ton)	M_{bd}	41.7
Blade length (m)	L_{bd}	86.4
Blade root diameter (m)	D_{bd}	3.54
Yoke weight (ton)	W_{yk}	50
Tugger line length (m)	L_d	10
1st rotational mode of blade about y-axis (Hz)	f_{r1}	0.08

equation [74], which is suitable for calculating forces on a slender structure [75]. The hydrodynamic force per unit length normal to each strip of monopile is given by

$$f_s = \rho C_M \frac{\pi D^2}{4} \ddot{x}_w - \rho(C_M - 1) \frac{\pi D^2}{4} \ddot{\eta}_1 + \frac{1}{2} \rho C_D D (\dot{x}_w - \dot{\eta}_1) |\dot{x}_w - \dot{\eta}_1|, \quad (1)$$

where ρ is the density of sea water, D is the diameter of the monopile, and C_M and C_D are the mass and drag coefficients, which are assumed as 2.0 and 1.0, respectively, in this study. Additionally, x_w describes the velocity, where \ddot{x}_w describe the acceleration of water particles at the strip centre. Similarly, η_1 and $\dot{\eta}_1$ are the velocity and acceleration of each strip, respectively.

3.1.2. Single blade-lift sub-system

The single blade-lift sub-system modelled in HAWC2 consists of a DTU 10 MW blade [71] that is 86.4 m long, a yoke added as a concentrated mass at the blades centre of mass, one lift wire, two sling wires and two tugger lines (Fig. 6). The parameters used in this study are based on previous work [7] and reported in Table 2. One end of the lift-wire is connected to the crane tip, which is modelled as fixed, whereas the other end of the lift wire is connected to sling wires. Furthermore, each tugger line is 10 m long, with one end attached to the crane boom, whereas the other is attached to the blade. Note that the attachment points of both the tugger lines are equidistant from the blades centre of mass and thus aid in restraining the lifted blade motion in the horizontal plane. The tugger lines are defined as cable bodies of length 1 m each and are connected by spherical joints to model their non-compressible nature [5]. The entire blade is modelled as flexible bodies, and the blade is aligned perpendicular to the wind direction.

The lifted blade is exposed to wind-induced loads, which in our study are calculated based on the Mann's turbulence module available in HAWC2. Mann's model [76] is characterised by its consideration of isotropic turbulence in a neutral atmosphere; however, it can also consider non-isotropic turbulence via the application of rapid distortion theory. Steady aerodynamic lift and drag parameters are utilised along with the cross-flow principle [77], which neglects the components of wind in the spanwise direction of the blade assuming the wind flow is 2D.

3.1.3. Tuned mass damper sub-system

The TMD device used in this study is a mass-spring-damper system with one degree of freedom. In practice, a steel cube can be used as the mass element, and elastomeric bearings as the spring element and rubber compound elements as a source of damping [78]. The device acts in the fore-aft (Y) direction of the monopile and this setup is chosen to investigate the effects of a TMD on the impact velocity in the y-direction, which is critical for sideways impacts at the blade root. Fig. 6 illustrates the position of the TMD sub-system installed inside the turbine tower structure. The reason for mounting the TMD in the turbine tower is twofold - first of all, it does not pose displacement constraints posed by nacelle given that nacelle have sensitive equipment, and secondly TMD system in tower can also aid during installation of nacelle along with blades (given that nacelle and blades are installed in sequence). This can be achieved by tuning the TMD to a specific frequency so that it can aid in the installation of nacelle first and then be re-tuned to a frequency relevant for installation of wind turbine blades. However, it is to be noted that the nacelle with generator inside is very heavy, and this will change the natural frequency of the system. This implies that in order to use a TMD for nacelle installation, the TMD should have the ability to change the natural frequency.

Fig. 7 presents the modelling procedure of a TMD system in HAWC2. The TMD system is implemented through an external force Dynamic Library Link (DLL) file written in Fortran. The TMD module is based on the work of [79], in which a two degree-of-freedom TMD system was developed for the ServoDyn module of FAST v8. Details of the formulation of the TMD system can be found in Ref. [79]. After the DLL file for TMD module is developed, it is then required to specify the node to which the TMD will be connected. Therefore, the original parameters of the monopile system contained in the HAWC2 input file (*.htc) are modified, and the TMD module is added; see Fig. 7. Furthermore, a TMD input file is also developed; this file consists of optimised parameters of the TMD, i.e., the mass ((M_y) , stiffness (k_y), damping ratio (ζ_y)) and initial position of TMD. The file is read when the TMD module interacts with HAWC2 during the simulation. Note that the computational procedure using the TMD formulation in HAWC2 utilises the global

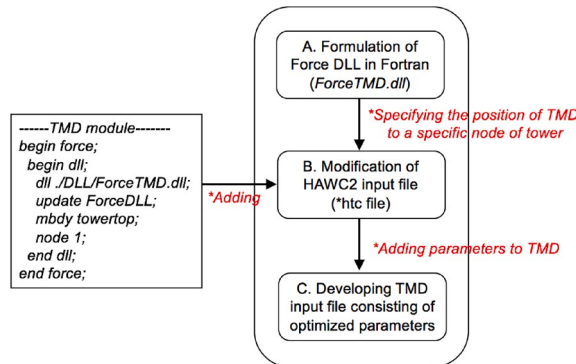


Fig. 7. Numerical modelling of tuned mass damper sub-system in HAWC2.

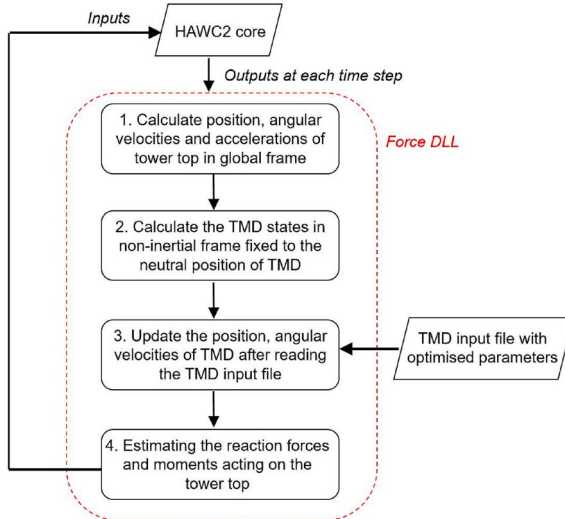


Fig. 8. Numerical procedure followed during interaction between HAWC2 and TMD.

inertial reference frame in addition to the non-inertial reference frame attached to the TMD neutral position; see Fig. 8. First, the HAWC2 outputs the original position, linear and angular velocities and accelerations of the tower top in the global reference frame. Then, it is transformed to the TMD states in the non-inertial frame. The TMD input parameters are read, and new TMD states are obtained.

Finally, the forces and moments acting on the tower top are fed into the HAWC2 main program.

The parameters of the TMD used in the study are optimised, and the details are summarised in Table 3. The mass of the TMD (M_y) is first obtained empirically corresponding to 2% of the structural weight of the monopile system, and then the value of stiffness (k_y) is adjusted accordingly such that the resulting eigenfrequency of the TMD matches the first fore-aft mode of the monopile system. Finally, the damping ratio (ζ_y) is calculated via a free decay test performed at the tower top, without any environmental load case. The total time for the decay test is considered as 200 s, in which a constant force is applied to the tower top for the first 50 s. The damping ratio is optimised by minimising the variance of the tower top displacement in the y -direction.

Fig. 9 presents the results of the free decay test with and without a TMD. It is seen that the addition of the TMD to the monopile system increases the damping ratio of the monopile system from 1% to 5.6%, and the displacement of tower top decreases significantly. Further, in the considered sea states, the maximum displacement of the tuned mass damper from its neutral reference position is 0.6 m which is less than the tower-top radius (2.75 m) of the DTU 10 MW wind turbine. Therefore, the mounting of TMD system is feasible in the turbine tower.

3.2. Environmental load cases

The impact velocity in the y -direction, which causes sideways impacts of the blade root with the hub, is the parameter of interest in this study. Table 4 lists the different environmental load cases considered in the paper to investigate the effects of a tuned mass damper. These environmental load cases correspond to different combinations of H_s , T_p , U_w and β_{wave} taken for the “North Sea Centre”, which is a representative offshore site for practical offshore wind farm installations. The water depth of the site is 29 m, which is close to the water depth of 30 m considered in this study. Fig. 10(a) presents the mean spectral peak period of wave (T_p) at the site from ten years of hindcast data, i.e. from 2001 to 2010 for several combinations of U_w and H_s . It can be clearly seen that for practical operational sea state ($H_s \leq 2$ m, and $U_w \leq 8$ m/s), waves with mostly low T_p ($T_p \leq 8$ s) occurs. Therefore, the site will have critical responses during blade mating process, given that most of the waves are close to the eigenfrequency of the monopile in the first fore-aft mode. Fig. 10(b) also presents a histogram of the spectral peak period of waves for the site and this clearly demonstrate the dominance of waves with

Table 3
Optimised parameters of the tuned mass damper (TMD).

Parameter	Value
M_y (kg)	62765
K_y (N/m)	142725
C_y (Ns/m)	15144
ζ_y (%)	8

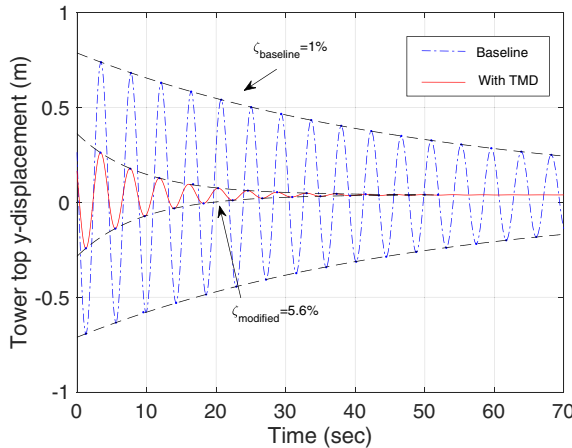


Fig. 9. Comparison of the free decay test performed at the tower top with and without TMD.

Table 4
Environmental load cases considered in this study.

EC	β_{wave}	H_s (m)	T_p (s)	U_w (m/s)
1	0°	1,1.5, ...,3.0	4,6, ...,12	8
2	30°	1,1.5, ...,3.0	4,6, ...,12	8
3	60°	1,1.5, ...,3.0	4,6, ...,12	8

low spectral peak periods ranging from 4 to 12 s. Therefore, this is the range of T_p considered in this paper for the analysis. In addition, the hindcast data for the site also reveal the wind-wave misalignment conditions varying mostly between 0 and 60°; see Fig. 10(c). Therefore, we consider three cases of wind-wave misalignments, i.e., $\beta_{wave} = 0, 30, 60$ degrees. Fig. 11 illustrates the bird view of wind-wave misalignment considered in this study with respect to blade installation process. Note that for all of the environmental conditions considered in the paper; see Table 4, $T_p = 4$ s matches closely with the eigenfrequency of the monopile in the first-fore aft mode and is expected to give very high hub motions. Further, each load case has ten 1000-s simulations with random seeds, out of which 400 s were removed to avoid any start-up effects. An average of 90% fractile maximum values for relative velocities between hub and blade root for each load case is considered as the impact velocity in this study. Note that the parameters considered in the analysis such as the time step increment and number of seeds are based on a sensitivity study, where computational efficiency and convergence of the standard deviations of the hub motions are checked.

3.3. Structural impact modelling of the blade root with hub

An impact assessment of the blade root is performed for the case in which a single T-bolt connection with a guide pin suffers a sideways impact with the hub during the mating process. The purpose of this analysis is to estimate an allowable level of impact velocity below which there is no critical damage at the blade root, which can deteriorate the blade's structural integrity. This threshold value will be utilised to estimate which environmental load cases are safe for mating wind turbine blades, considering the installation task with and without a TMD. In this manner, the efficiency of a TMD device on the overall operability of a mating operation can be quantified. Note that in principle, there is a possibility that more than one bolted connection impacts the hub during mating. However, we consider the case of a single guiding connection impacting the hub because this assumption neglects any impact force distribution with adjacent connections and is thus conservative.

We utilise the Abaqus/explicit [80] environment for this purpose, given that the solver scheme is efficient at treating nonlinear numerical problems involving complex interactions, in addition to large rotations and deformations [81]. The DTU 10 MW blade [71] is considered as the base model for the impact analysis. The reference blade is 86.4 m long, with a root diameter of 5.4 m and is based on shell elements. To perform the impact assessment of the blade root considering the guide pin, a high-fidelity local solid part is separately modelled as a T-bolt connection and is connected with the remaining DTU 10 MW blade using the shell-to-solid coupling method (Fig. 12). The shell-to-solid coupling method is a technique that enables the coupling of a high-fidelity local solid model of a structure requiring detailed investigation with the shell elements of a structure that mainly contributes to inertia.

Fig. 12 presents the finite element model of the local solid part developed using advanced capabilities of Abaqus with a python-based scripting interface. The dimensions of the local solid part are taken from Ref. [7]. The local solid part consists of a root laminate modelled as a homogenised triaxial material with layup [+45/-45/0] having a thickness of 100 mm, a steel barrel nut having a diameter 56 mm, and a steel guide pin bolt of diameter 28 mm and length 400 mm. The threaded connection at the barrel nut and guide

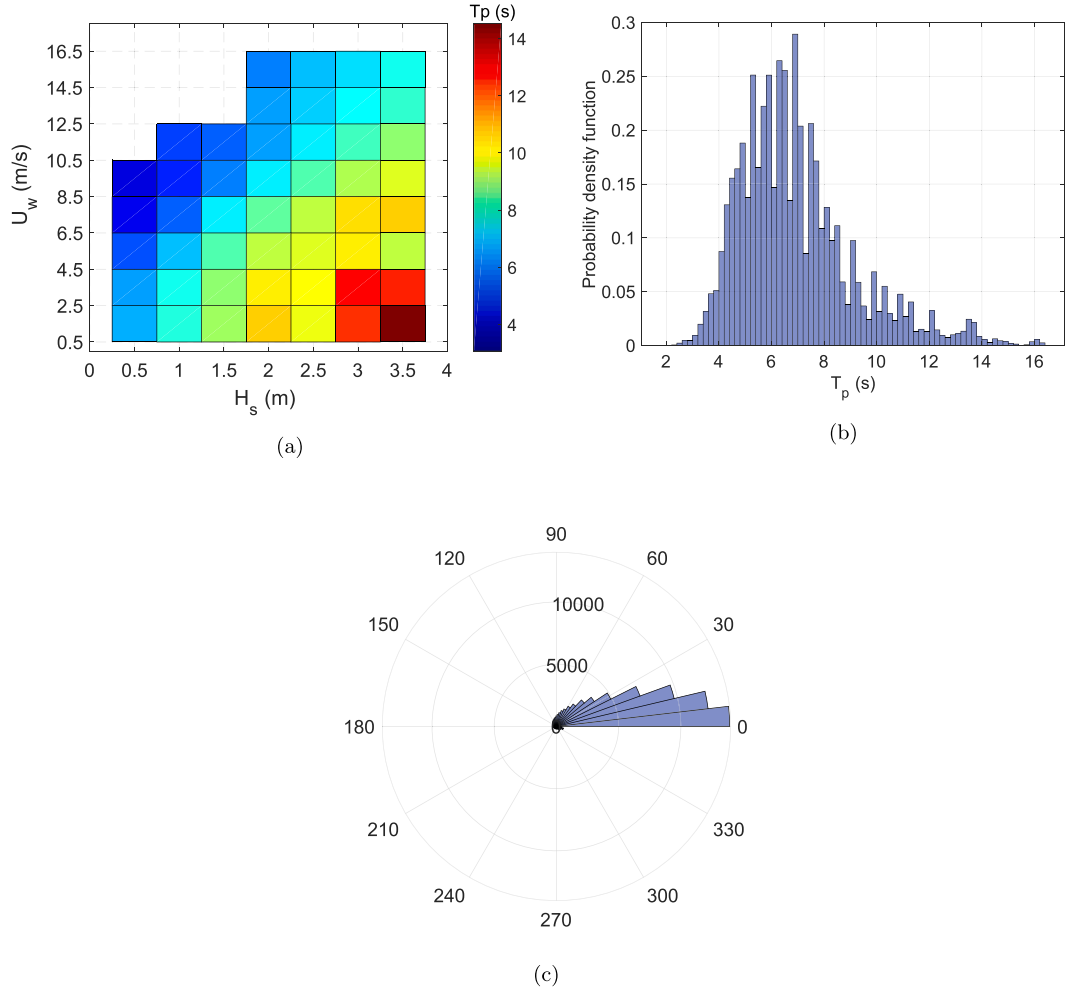


Fig. 10. Hindcast data for ‘North sea centre’ site for duration of 10 years 2001–2010 (a) Mean T_p for various wind and wave combinations (b) Histogram distribution of T_p (c) Polar rose diagram of misalignment between wind-wave.

pin assembly is neglected, and the bolt head is appended onto the barrel nut by using the tie-constraint technique available in Abaqus. The tie-constraint technique enables two different parts in a structure to behave as rigidly connected with each other during the analysis. The guide pin bolt is inserted through an in-plane hole in the root laminate, which has a diameter slightly larger than the diameter of the guide pin. No initial contact pairs between the bolt and the laminate along the in-plane hole are available; however, contact interaction properties are defined between them in the finite element model. This is because of potential contact between the laminate and bolt during impact. Furthermore, the barrel nut is assembled into the transverse hole of the root laminate, and contact interaction properties are defined between the barrel nut and laminate in the hole. The general contact scheme available in Abaqus/explicit is applied, in which a hard contact pressure over-closure and frictionless behaviour is defined as the interaction property. The entire local solid part was discretised with brick elements having eight nodes and a reduced integration scheme (C3D8R), with an element size of 5.6 mm chosen based on a mesh convergence study, which is described in Ref. [7]. The remainder of the blade was modelled with conventional 4-node thick shell S4R elements. Furthermore, a generalised geometrical representation of the hub is considered and modelled as a rigid body with 4-noded bilinear R3D4 elements, having diameters of 6 m, and is constrained in all degrees of freedom. A hard-contact interaction behaviour with a coefficient of friction of 0.3 was assigned between the guide pin bolt at the contact region Y'Y' with the hub in the sideways direction; see Fig. 12. Note that the sideways impact corresponds to the x-direction of the structural coordinate system (xyz) in the finite element calculation performed in Abaqus. Finally, different impact velocities (V_x^{fem}) ranging between 0.1 m/s and 1 m/s ($0.1 \leq V_x^{fem} \leq 1$) are considered to find the threshold level of impact velocity, below which there is no critical damage at the blade root.

3.4. Constitutive material models

The local solid part consists of a homogenised triaxial material for the root laminate and steel material for the barrel nut and guide

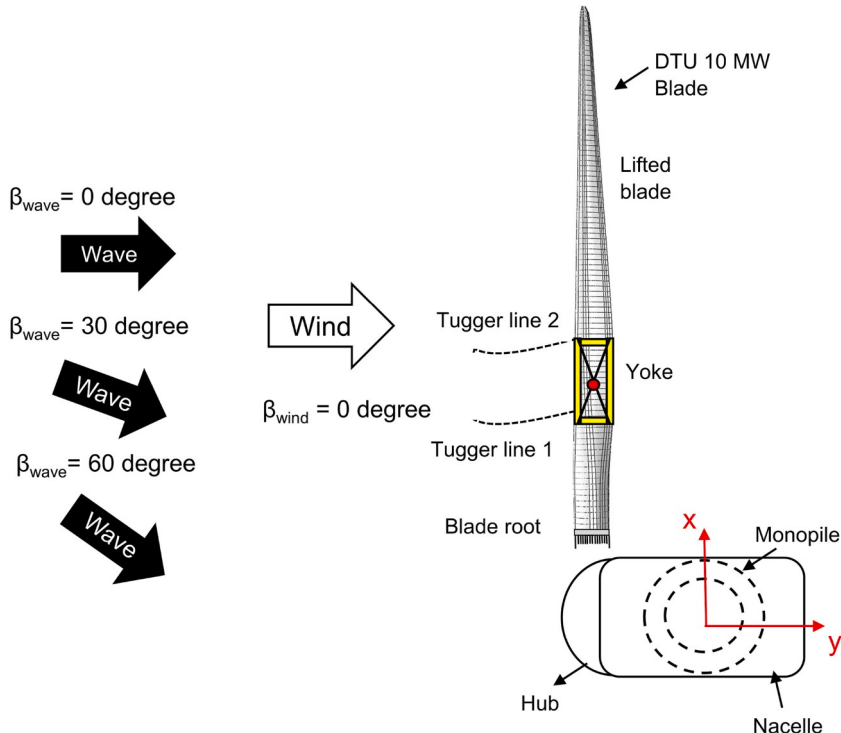


Fig. 11. Bird view illustrating wave-wind misalignment condition with respect to blade mating process.

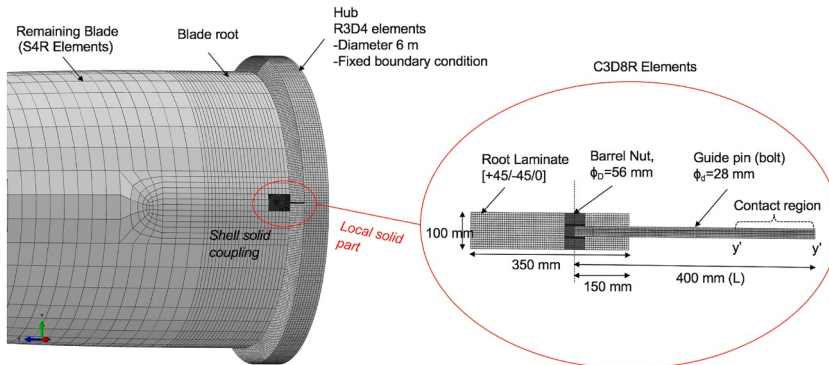


Fig. 12. Finite element modelling at the blade root.

pin bolt. We utilise two separate constitutive material models for estimating failure in the root connection due to impact; these models are discussed below.

3.4.1. Maximum stress failure criterion

The maximum stress criterion is utilised for predicting failure in the composite root laminate. The criterion is simple and is widely utilised methods [82]; however, it does not consider interaction between different stresses into consideration, and damage cannot be predicted progressively. Nevertheless, in this article, the main aim is to estimate the impact velocity at which damage occurs to the root laminate due to impact, and thus a progressive failure analysis is beyond the scope of this paper. Failure is predicted by a single parameter, the 'Failure index' F_I [7], exceeding the value 1; this index is defined as

F_I

$$F_I = \max \left\{ \begin{array}{l} |F_1(S_{11})|; \text{ where } F_1(S_{11}) = \begin{cases} \frac{\sigma_1}{X^T} & \text{if } \sigma_1 > 0 \\ \frac{\sigma_1}{X^C} & \text{if } \sigma_1 < 0 \end{cases} \\ |F_1(S_{22})|; \text{ where } F_1(S_{22}) = \begin{cases} \frac{\sigma_2}{Y^T} & \text{if } \sigma_2 > 0 \\ \frac{\sigma_2}{Y^C} & \text{if } \sigma_2 < 0 \end{cases} \\ |F_1(S_{33})|; \text{ where } F_1(S_{33}) = \begin{cases} \frac{\sigma_3}{Z^T} & \text{if } \sigma_3 > 0 \\ \frac{\sigma_3}{Z^C} & \text{if } \sigma_3 < 0 \end{cases} \\ |F_1(S_{12})|; \text{ where } F_1(S_{12}) = \begin{cases} \frac{\sigma_{12}}{S_{12}^t} & \text{if } \sigma_{12} > 0 \\ \frac{\sigma_{12}}{S_{12}^l} & \text{if } \sigma_{12} < 0 \end{cases} \\ |F_1(S_{13})|; \text{ where } F_1(S_{13}) = \begin{cases} \frac{\sigma_{13}}{S_{13}^t} & \text{if } \sigma_{13} > 0 \\ \frac{\sigma_{13}}{S_{13}^l} & \text{if } \sigma_{13} < 0 \end{cases} \\ |F_1(S_{23})|; \text{ where } F_1(S_{23}) = \begin{cases} \frac{\sigma_{23}}{S_{23}^t} & \text{if } \sigma_{23} > 0 \\ \frac{\sigma_{23}}{S_{23}^l} & \text{if } \sigma_{23} < 0 \end{cases} \end{array} \right\} \quad (2)$$

where σ_1 and σ_2 are in-plane normal stresses, σ_3 is the transverse normal stress, σ_{12} is the in-plane shear stress, and σ_{13} and σ_{23} are interlaminar shear stress. The final failure index is the maximum value of the modulus of the individual failure index values $|F_1(S_{ij})|$. Note that the strength values used in the equations given by X^T , X^C , Y^C , Y^T , Z^T , Z^C , S_l^{12} , S_l^{23} , and S_l^{13} have varying values in different material orientations of the laminate coordinate system, in addition to different values in the tensile and compressive directions of stresses. These values were derived from the literature, correspond to manufacturer data [83] and are reported in Table 5.

3.4.2. von Mises criterion with equivalent plastic strain

A standard-grade 8.8 steel is used in this study for the M28 guide pin bolt and the barrel nut. A von-Mises stress and equivalent plastic strain criterion is used to model damage in the steel. An isotropic hardening model is utilised for defining the plastic properties, where the data points for the true stress-logarithmic plastic strain are calibrated from the engineering stress strain curve derived from Ref. [84]. The material properties of the steel utilised in this study are listed in Table 5.

4. Results and discussions

In this section, response-time histories, spectral densities, and response statistics are compared for installation systems with and without the tuned mass damper (TMD). The effectiveness of the TMD is discussed first in terms of hub motions and impact velocities developed between root and hub in the global y-direction. Then, the finite element results for the impact assessment at the blade root are presented, and the threshold velocity of impact is determined. The impact velocities obtained for different load cases are related with sea state parameters using the response surface method, and the operational limiting envelopes for the mating process are derived. Note that to consider statistical uncertainty during the dynamic response calculation, an average of ten seeds are considered.

Table 5
Material properties implemented for finite element analysis [7,83].

Property	Symbol	Value	Units
Composite laminate			
Density	ρ	1864.0	kg/m^3
Young's Modulus	$E_1; E_2; E_3$	21.69; 14.67; 12.09	GPa
Shear Modulus	$G_{12}; G_{23}; G_{13}$	9.413; 4.53; 4.53	GPa
Poisson's Ratio	$\nu_{12}; \nu_{13}; \nu_{23}$	0.478; 0.275; 0.3329	–
Longitudinal strength	$X^T; X^C$	472.06; 324.16	MPa
Transverse strength	$Y^T; Y^C$	127.1; 127.1	MPa
Through thickness strength	$Z^T; Z^C$	38.25; 114.7	MPa
Shear strength	$S_{12}^t; S_{13}^t; S_{23}^t$	99.25; 78.21; 39.51	MPa
Steel			
Density	ρ	7850	kg/m^3
Young's Modulus	E	210	GPa
Poisson's Ratio	ν	0.3	–

4.1. Hub motions

The mating process includes attachment of the blade root with the hub. The hub is located at the topmost position of the turbine, and its responses are governed by wave-induced action on the monopile. The efficiency of the TMD during the mating process depends on its ability to reduce hub motions. Table 6 lists the standard deviations of the displacement of the hub in the global y-direction for different wave spectral peak period values ($T_p = 4 \text{ s}, \dots, 12 \text{ s}$) considered for system with and without the TMD (baseline). These results correspond to a significant wave height ($H_s = 2 \text{ m}$) and collinear wave-wind conditions ($\beta_{\text{wave}} = 0^\circ$). It can be observed that the hub motions, irrespective of whether the TMD is installed, are greatest when close to $T_p = 4 \text{ s}$ and decrease with increased T_p . For example, as can be observed in the table for installation system without the TMD (baseline), the standard deviation of the hub motion in the y-direction at $T_p = 4 \text{ s}$ is 0.48 m, which decreases to 0.086 m at $T_p = 12 \text{ s}$.

This result is due to the resonance-driven monopile motion because the eigenperiod of the monopile in the first fore-aft mode (T_{FA}) is 4.2 s; the resonance effect further decreases as the wave spectral peak period becomes more different from the resonance frequency. The table also clearly indicates the effect of the TMD at reducing hub motion, as the column with STD^{TMD} has significantly lower values than STD^{baseline} for a particular T_p . For example, the standard deviation of hub motion at $T_p = 4 \text{ s}$ for the baseline model is 0.48 m, which decreases to 0.172 m for the installation system with the TMD. Thus, the TMD abbreviates the motion of the hub by more than 64%. However, the effectiveness of TMD for hub motions is highest at lower T_p , close to the eigenperiod of monopile in first fore-aft mode and decreases with increased T_p , as seen in the last column, where the relative reduction in the hub motions due to the TMD is presented. The % relative reduction reduces from 64.16% at $T_p = 4 \text{ s}$ to 52.32% at $T_p = 12 \text{ s}$. This observation is in line with the previous results reported in Ref. [6].

Fig. 13(a) further presents the comparison of motion of hub-centre in the xy-plane for the installation system with and without the tuned mass damper considering an environmental load case with $H_s = 1.5 \text{ m}$, $T_p = 6 \text{ s}$ and $\beta_{\text{wave}} = 0^\circ$. It can be observed that the motion of the hub centre in the y-direction is significant compared to its motion in the x-direction. The hub-centre displacement in the y-direction reaches a maximum of 0.8 m, whereas the motion in the x-direction is negligible. This result implies that the sideways impact of the blade root with the hub is a critical impact scenario for collinear wave-wind condition ($\beta_{\text{wave}} = 0^\circ$). Additionally, the tuned mass damper, which acts in the fore-aft direction, reduces the motion of the hub-centre in y-direction by more than 60%, as indicated by the red curve in Fig. 13(a). Fig. 13(b) presents the spectral density curve for the hub motion in the y-direction; there are two frequency peaks observed. One corresponds to the wave frequency ($T_p = 6 \text{ s}$, 0.166 Hz), whereas the other corresponds to the eigenfrequency of monopile in the first fore-aft mode, which is approximately 0.24 Hz. It can be clearly seen that the TMD reduces only the peak of the eigenfrequency contributed from first fore-aft mode of the monopile. Additionally, since the motion of hub is predominantly in the y-direction, the velocity of the hub centre in this direction will contribute substantially to the impact velocity between root and hub in the y-direction. Fig. 13(c) presents a comparison of hub velocity in the global y-direction with and without the TMD, which distinctly shows the effectiveness of the TMD at reducing the velocity of the hub. Similar observations are seen in the spectrum of the velocity of hub centre shown in Fig. 13(d), where only the frequency peak contribution from the monopile motion is attenuated.

Fig. 14(a) and (b) further present the effects of wind-wave misalignment (β_{wave}) on the motion of hub-centre in the xy-plane and the effectiveness of tuned mass damper in reducing the hub motions. The environmental load case with $H_s = 1.5 \text{ m}$, $T_p = 6 \text{ s}$ and $\beta_{\text{wave}} = 30^\circ, 60^\circ$ is considered here for discussion. It can be observed that unlike the collinear wave-wind condition ($\beta_{\text{wave}} = 0^\circ$, Fig. 14(a)), in which the dominant motion of the hub centre lies explicitly in the y-direction, for wind-wave misalignment conditions, the motions of hub centre are considerable in both the x- and y-directions and are correlated. However, for $\beta_{\text{wave}} = 30^\circ$ and 60° , the motions of hub centre in the y-direction are significantly less than for $\beta_{\text{wave}} = 0^\circ$. For the same environmental load case, for $\beta_{\text{wave}} = 0^\circ$, the response maximum for hub motion in the y-direction reaches 0.8 m, compared to $\beta_{\text{wave}} = 30^\circ$, where the motion of hub in y-direction is slightly greater than 0.3 m. Additionally, since the motions are correlated, the TMD reduces the overall hub motions in the xy-plane, as can be observed from the inclined nature of red curve shown in Fig. 14(a) and (b) compared to the straight-line attenuation of the hub motion by the TMD for the collinear wind-wave direction ($\beta_{\text{wave}} = 0^\circ$) shown in Fig. 13(a).

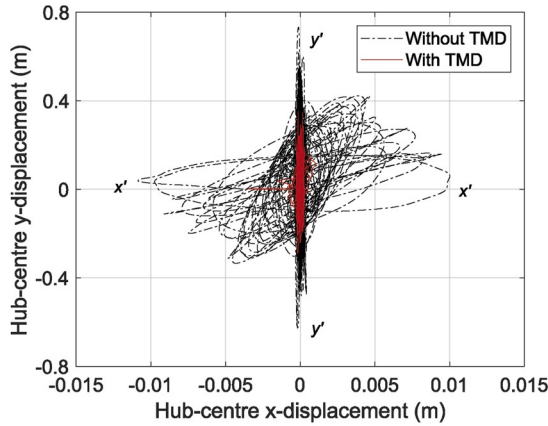
4.2. Blade root motion

To obtain the characteristic relative impact velocity between blade root and hub, it is important to understand the motion of the blade root during the mating phase, which is caused by action of wind induced loads. Fig. 15(a) presents the response time histories for velocity of blade root in the y-direction for the case in which $U_w = 8 \text{ m/s}$. Since the damper system is installed explicitly in the

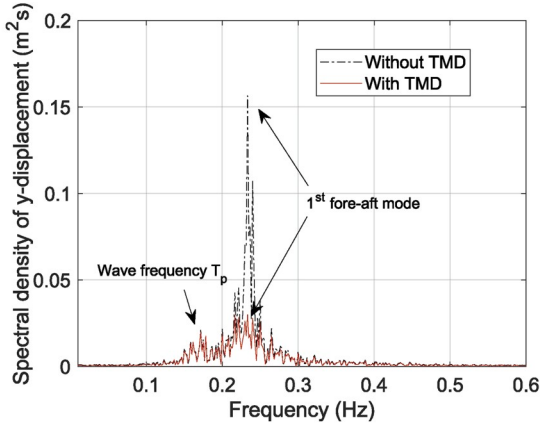
Table 6

Standard deviations of the hub displacement in the global y-direction, $H_s = 2 \text{ m}$ and $\beta_{\text{wave}} = 0^\circ$.

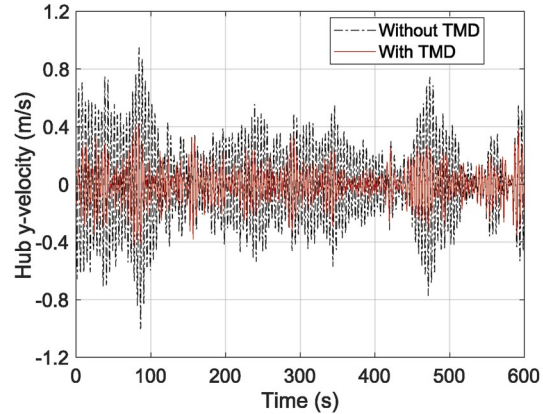
$T_p(\text{s})$	$STD^{\text{baseline}} (\text{m})$	$STD^{\text{TMD}} (\text{m})$	$\frac{STD^{\text{TMD}} - STD^{\text{baseline}}}{STD^{\text{baseline}}} (\%)$
4	0.48	0.172	-64.16
6	0.29	0.11	-62.06
8	0.175	0.072	-58.85
10	0.12	0.054	-55.00
12	0.086	0.041	-52.32



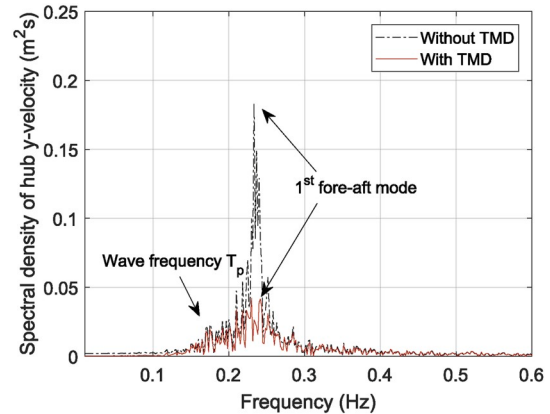
(a)



(b)

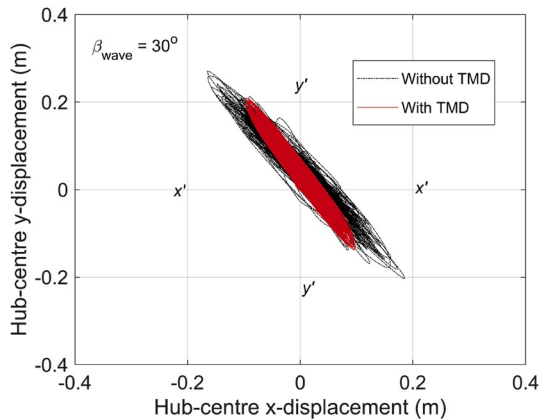


(c)

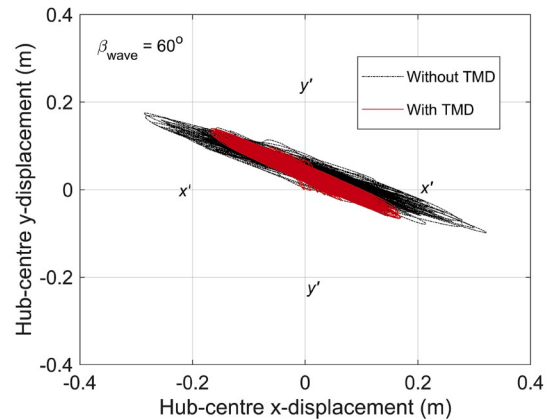


(d)

Fig. 13. Comparison of responses with and without TMD for $H_s = 1.5$ m, $T_p = 6$ s, $\beta_{wave} = 0^\circ$ (a) Hub-centre displacement (xy plane) (b) Spectrum of hub-centre y-displacement (c) y-velocity of hub, and (d) Spectral density of hub y-velocity.



(a)



(b)

Fig. 14. Comparison of hub-centre motion in xy plane with and without TMD and varying wind-wave misalignment condition for $H_s = 1.5$ m, $T_p = 6$ s (a) $\beta_{wave} = 30^\circ$ (b) $\beta_{wave} = 60^\circ$.

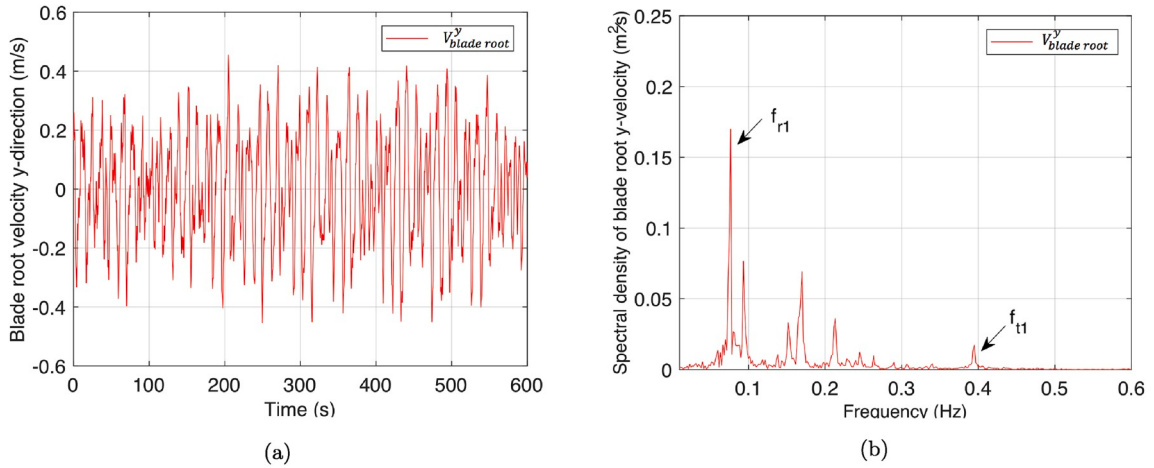


Fig. 15. (a) Blade root y-velocity (b) Spectral density of blade root y-velocity ($U_w = 8 \text{ m/s}$).

monopile subsystem, there is no effect on the dynamic motion response of the blade root, and the curves completely overlap. The velocity of the blade root reaches a response maximum of 0.42 m/s, which is significant; however, this value is less than the velocity of the hub centre in the y-direction shown previously. The spectrum of the blade root velocity shown in Fig. 15(b) presents different peaks, with the maximum peak occurring at approximately 0.08 Hz, which is the 1st rotational mode of the blade about the global y-axis. It is also worth mentioning that the motion of the blade root and its velocity are negligible in the global x-direction due to the action of tugger lines.

4.3. Impact velocity

The most relevant parameter for blade root impact with the hub during the mating process, which decides the consequence of an impact event is the impact velocity developed between them in the global y-direction. Fig. 16(a) presents the response time-history for impact velocity in y-direction for a case with $H_s = 1.5 \text{ m}$, $T_p = 6 \text{ s}$, $\beta_{\text{wave}} = 0^\circ$, and $U_w = 8 \text{ m/s}$. It is found that for this case, the tuned mass damper reduces the response maximum of the impact velocity between the root and hub by more than 40%. Note that the efficiency of the TMD in reducing impact velocity is relatively lesser compared to its efficiency in exclusively reducing the hub velocity, see Fig. 13(c).

This is because the blade root velocity in the y-direction contributes significantly to the impact velocity; however, it is not attenuated by the TMD. The spectrum curve for the impact velocity shown in Fig. 16(b) also supports this argument as different peaks corresponding to the blade's 1st rotational mode (f_{r1}), wave frequency, eigenfrequency of the monopile in first fore-aft mode, and blade translational mode (f_{t1}) are seen; however, the tuned mass damper (TMD) only reduces the peak frequency contributed by the monopile motion in the first fore-aft mode.

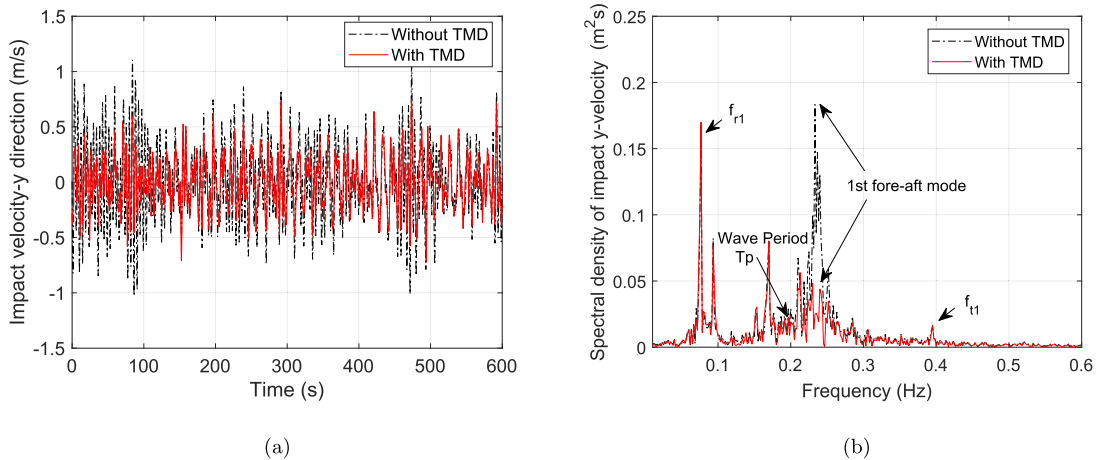


Fig. 16. (a) Reduction of impact velocity y-direction with tuned mass damper (b) Spectral density of impact velocity y-direction with and without TMD ($H_s = 1.5 \text{ m}$, $T_p = 6 \text{ s}$, $\beta_{\text{wave}} = 0^\circ$, and $U_w = 8 \text{ m/s}$).

Fig. 17(a)-(c) present the impact velocities in the y-direction developed between blade root and hub for installation system with and without TMD, for different wind-wave misalignment conditions ($\beta_{wave} = 0^\circ, 30^\circ, 60^\circ$) for $H_s = 1.5$ m, $T_p = 4, 6, \dots, 12$ s, and $U_w = 8$ m/s. For all β_{wave} , the impact velocities are highest at low T_p and decrease further with increasing peak period. The impact velocity for the baseline model without TMD at $\beta_{wave} = 0^\circ$ at $T_p = 4$ s is 2.3 m/s, whereas at $T_p = 12$ s, it reduces to 0.79 m/s. A similar trend is observed for the attenuated value for the installation system with TMD, where maximum impact velocities are observed at $T_p = 4$ s, which is close to the eigenfrequency of the monopile in the first fore-aft mode and then reduces further with increasing peak period of the wave. Further, the absolute value for impact velocity in y-direction at a given peak period is highest for $\beta_{wave} = 0^\circ$ and reduces further with increase in wind-wave misalignment conditions. For example, as seen in Fig. 17(a) and (c), respectively, the impact velocity for $H_s = 1.5$ m, $T_p = 4$, and $\beta_{wave} = 0^\circ$ is 2.3 m/s, which reduces to 1.4 m/s at $\beta_{wave} = 60^\circ$.

To obtain an analytical relationship between impact velocity in the y-direction and sea state parameters H_s and T_p , response surface method (RSM) is utilised. The RSM method [85] is an ensemble of different mathematical and statistical techniques where an analytical expression can be obtained for a response variable which is dependent on many independent variables. Fig. 18(a)-(c) present the comparison between response surfaces (RSs) with and without TMD, estimated for impact velocity in the y-direction for different environmental load cases with $\beta_{wave} = 0^\circ, 30^\circ$, and 60° and $U_w = 8$ m/s. Note that for each response surface, there were 25 points (5x5, combination between 5 values for H_s and 5 values for T_p) fitted for linear, quadratic, cubic, and quartic models with parameters such as root mean square error (RMSE) and coefficient of determination (R^2) checked for accuracy. The quartic model performed a best fit for the response surface and had 15 terms.

It can be seen from Fig. 18(a)-(c) that for all the cases of β_{wave} , the response surface for the installation system with TMD is smaller than for the baseline case without TMD. This result implies that the TMD is effective in reducing the impact velocities that can cause

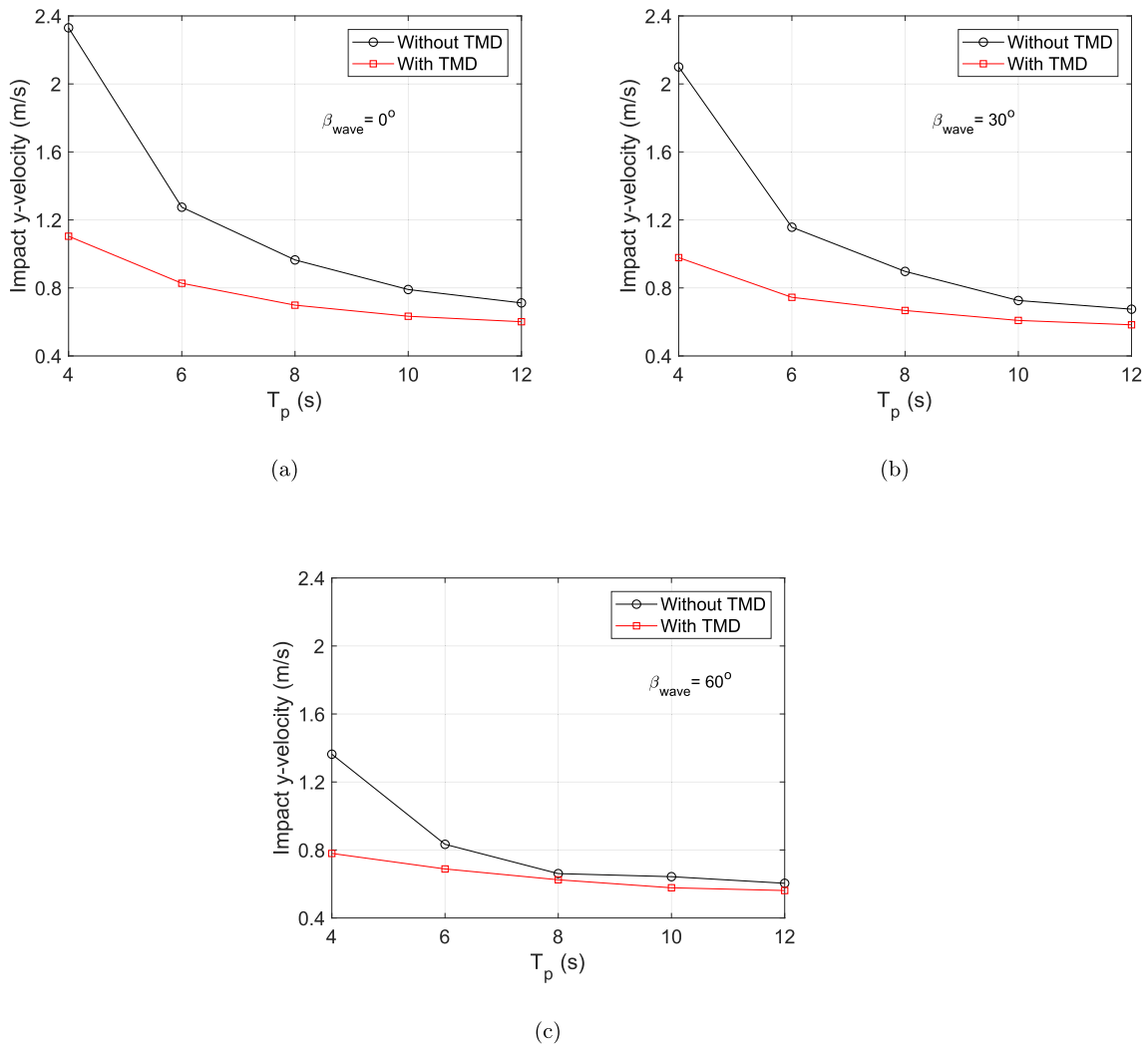


Fig. 17. Comparison of impact velocity y-direction with and without TMD for varying T_p considered for (a) $\beta_{wave} = 0^\circ$ (b) $\beta_{wave} = 30^\circ$ (c) $\beta_{wave} = 60^\circ$.

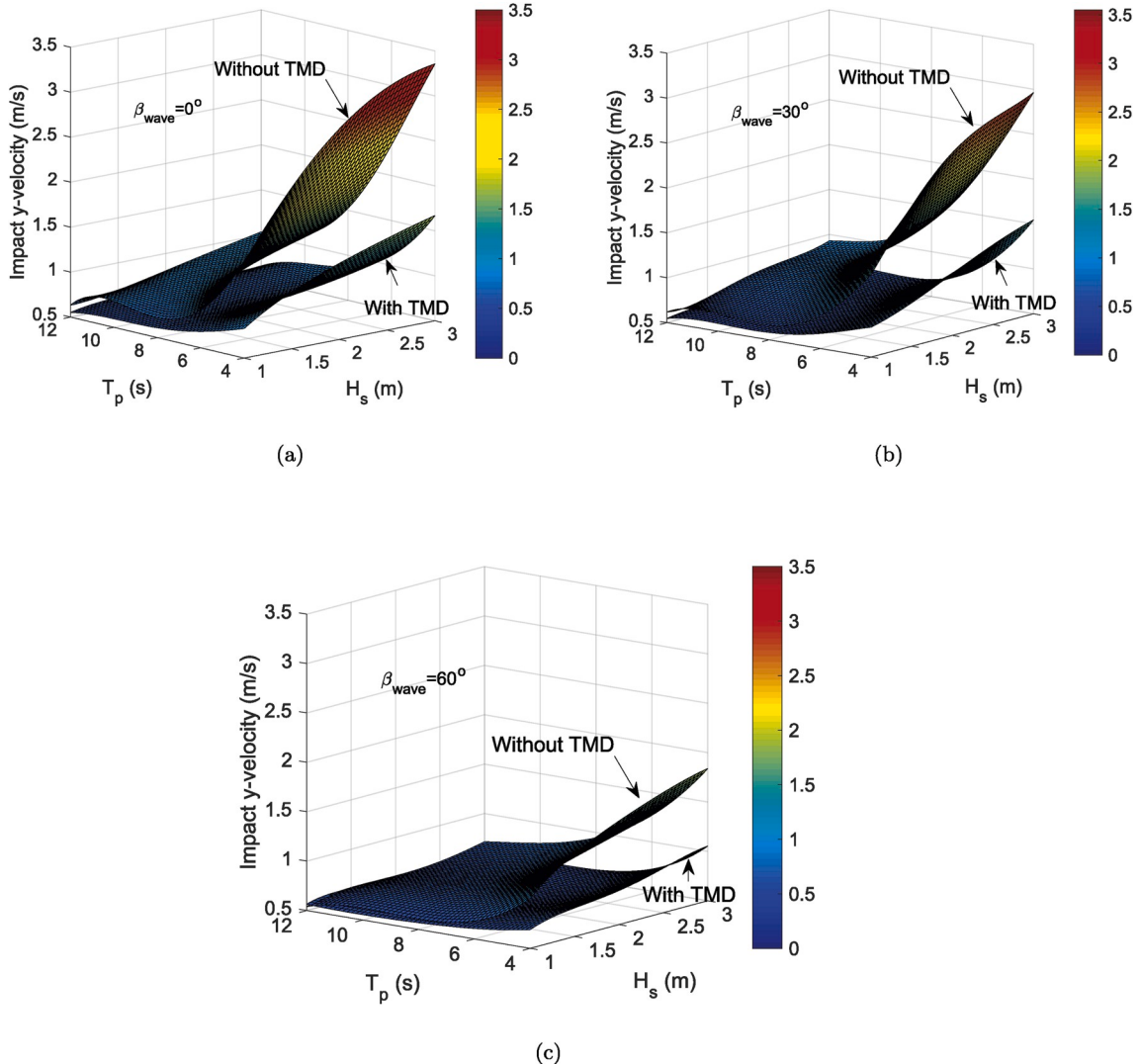


Fig. 18. Response surface comparison for impact velocity y-direction for installation system with and without TMD for (a) $\beta_{\text{wave}} = 0^\circ$ (b) $\beta_{\text{wave}} = 30^\circ$ (c) $\beta_{\text{wave}} = 60^\circ$.

sideways impact between root and hub. For example, from the response surface shown in Fig. 18(a), which corresponds to $\beta_{\text{wave}} = 0^\circ$, the impact velocity at $H_s = 3$ m and $T_p = 4$ s without tuned mass damper can reach an impact velocity of 3.4 m/s, which reduces to 1.7 m/s with TMD, which is more than 50% effectiveness in reducing impact velocity.

Further, it can be seen from the RSs that for higher T_p , away from the resonance frequency of the monopile in the first fore-aft mode, the difference in the range of impact velocities with and without TMD reduce. Therefore, it can be implied that for all β_{wave} , the impact velocities are reduced substantially by utilising tuned mass damper (TMD) which is significant at lower spectral peak period of waves. It is also clearly seen from the figure that the RSs for impact velocity are highest for collinear wave-wind conditions ($\beta_{\text{wave}} = 0^\circ$), and as the wind-wave misalignment increases the RS for the impact velocity reduces. As seen in Fig. 18(a)–(c) explicitly that the RS for $\beta_{\text{wave}} = 0^\circ$ is the largest while the RS for $\beta_{\text{wave}} = 60^\circ$ is the smallest. This is true for both the installation systems, i.e. with and without TMD.

Furthermore, to quantify the effectiveness of a TMD on the impact velocity developed between root and hub in the y-direction, a parameter percentage reduction (%) is defined, which is given by

$$\text{Percentage reduction}(\%) = \frac{V_y^{\text{TMD}} - V_y^{\text{baseline}}}{V_y^{\text{baseline}}} \times 100 \quad (3)$$

where V_y^{TMD} is the impact velocity obtained with TMD, whereas V_y^{baseline} is the impact velocity obtained for the baseline installation system without any tuned mass damper. Fig. 19(a)–(c) present the percentage reduction in impact velocity in y-direction for different load cases with $\beta_{\text{wave}} = 0^\circ$, $\beta_{\text{wave}} = 30^\circ$, and $\beta_{\text{wave}} = 60^\circ$ respectively. For $\beta_{\text{wave}} = 0^\circ$ and $T_p = 4$ s (Fig. 19(a)), the efficiency of TMD at

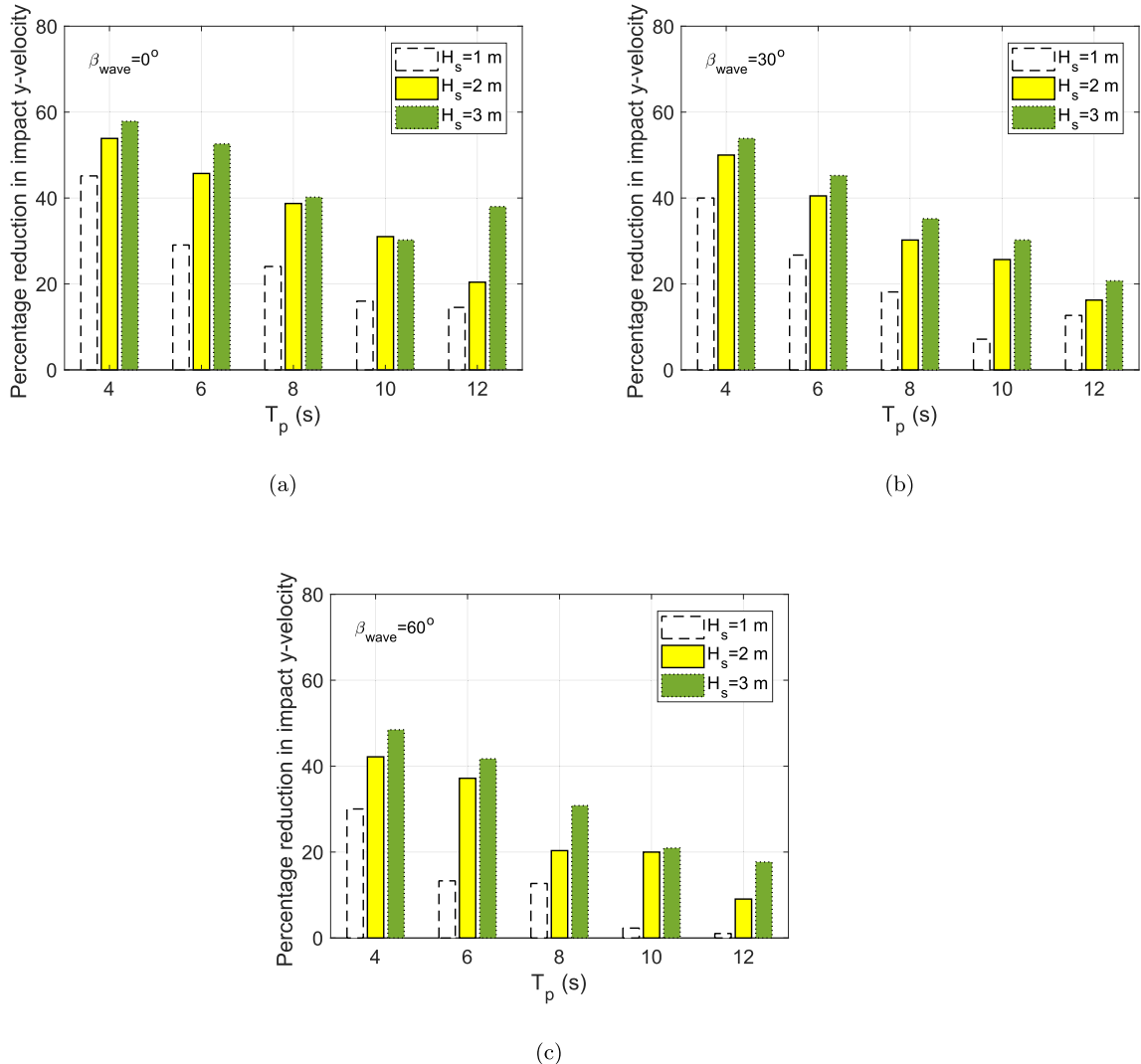


Fig. 19. Efficiency of TMD in reducing impact velocity for various load cases (a) $\beta_{wave} = 0^\circ$ (b) $\beta_{wave} = 30^\circ$ (c) $\beta_{wave} = 60^\circ$.

$H_s = 1 \text{ m}$ is 44%, which increases to 58% for $H_s = 3 \text{ m}$. Similar trends are observed for other β_{wave} , where the effectiveness of TMD increases with increasing H_s . Furthermore, the efficiency of TMD at $H_s = 3 \text{ m}$ drops from 58% at $T_p = 4 \text{ s}$ to 38% at $T_p = 12 \text{ s}$. Therefore, this implies that the effectiveness of tuned mass damper reduces with increasing T_p further away from the tuned frequency. When comparing the effectiveness of TMD with wind-wave misalignment condition, it can be seen from Fig. 19(a) and (c) respectively that for $H_s = 1 \text{ m}$, and $T_p = 4 \text{ s}$, the value reduces from 44% at $\beta_{wave} = 0^\circ$ to 30% at $\beta_{wave} = 60^\circ$. A similar observation is found for other load cases, and thus, it can be implied that the efficiency of TMD on the impact velocity reduces with increasing wind-wave misalignment conditions.

4.4. Effect of TMD on response-based limiting sea states

The planning phase is one of the important elements for any offshore installation activity. It involves the selection of suitable operational limiting sea states based on which, for a particular offshore site and duration of the activity, a weather window of operation is selected. In principle, these limits must consider the critical events that can cause failure of the installation activities, thus ensuring safe installation. In this article, a sideways impact of the blade root with the hub is referred to as a critical event. Hence, to discuss the competence of TMD, it is imperative to compare response based limiting sea states for mating process derived for installation system with and without TMD.

The primary step requires estimation of an allowable impact velocity (V_{allow}) for the critical event below which there are no critical damages developed at the blade root. This allowable value of impact velocity will be utilised to derive sea states from the response surfaces obtained for impact velocity. In this part of the paper, we first present results of the finite element analysis and determine the

allowable level of impact velocity, also referred to as threshold level. Then, the limiting sea states for installation system for different wind-wave misalignment conditions will be presented. It is further important to note that in the finite element analysis, a sideways impact corresponds to an impact velocity in the x -direction (V_x^{fem}) of the structural coordinate system.

4.4.1. Estimation of allowable velocity of impact (V_{allow})

Finite element analyses are carried out for the case where a single guide pin bolt at the blade root suffers a sideways impact with the hub. Different impact velocities ranging between 0.1 m/s to 1 m/s are considered. The energy conservation histories are checked after the analyses and it is confirmed that the numerical model gives stable results.

[Fig. 20](#) presents the result for a case where a guide pin at the blade root suffers an impact with the hub at $V_x^{fem} = 0.85 \text{ m/s}$. It can be seen that due to the impact, severe bending in the guide pin occurs which corresponds to an angle of around 12° with the initial state. Different categories of failure modes at the blade root connections were presented in Refs. [7,86] and it was shown that the bending of guide pin bolt alone is not a critical failure mode for the blade's structural integrity, as the guide pin can be reinstated with a new one by hoisting lifted blade back to the deck of the vessel. In this manner, another mating trial can be performed. Again, no plastic strains are developed in the barrel nut, which implies no damage in the barrel nut. However, due to the excessive impact-induced plastic deformation of the guide pin, an impact occurs between the bolt and root laminate. Since the contact interaction property is defined between the laminate and the guide pin bolt during the finite element modelling and constitutive material model is defined for the root laminate, the failure in the composite laminate can be quantified.

The stresses developed in the root laminate at the inplane hole due to impact with the steel bolt is investigated. It is found that the inplane normal (σ_{11}, σ_{22}) and inplane shear stresses (σ_{12}) at the inplane holes are found within the allowable values, and thus the failure index of these stresses are found in the range ($-1, 1$). However, large through-the-thickness tensile and compressive normal stresses along with transverse shear stresses are developed, and exceeds the allowable values presented in [Table 5](#). [Fig. 21](#) presents the corresponding failure index obtained for out-of-plane transverse normal stresses (σ_3) and interlaminar shear stresses (σ_{23}). It can be clearly seen that FI-S33 and FI-S23 have an index greater than 1 which clearly signifies the development of failure at the root laminate. As discussed before and described in Ref. [86], any damage to root laminate is defined as a critical failure mode, owing to the fact that composite laminates are susceptible of developing complex interacting failure modes due to impact, especially delamination and have potential to further grow, in case the damaged blade is installed onto the turbine. Therefore, such damage, if developed during mating task, will require critical repair work at the offshore site and can significantly delay the installation task, and it thus must be avoided. Again, the choice of a suitable damage criteria for estimating allowable impact velocity depends upon the consequence of the failure event, and is governed by the magnitude of risk installation contractor takes during the planning stage. A very stringent structural criterion is expected to put a strict cap on the weather window for installation, which is not favored in practice. In this study, an impact velocity that causes a failure mode that includes plastic deformation of guide pin and no damage to the root is considered as the allowable response parameter for determining the operational limit and is based on industrial discussions [17]. Since, the impact velocity of 0.85 m/s predicts failure at the root laminate, it is therefore implied that the threshold level would lie somewhere below this value. Several impact velocities are considered based on trial and error approach, with a target of obtaining an impact velocity where the failure index only manages to reach a value of 1. [Fig. 22](#) presents the absolute failure index developed in the root laminate for different cases of impact velocities, and it was found that 0.76 m/s is the threshold level of impact velocity where the failure index lies just below 1, implying that there is no damage predicted at the root laminate. Thus, $V_x^{fem} = 0.76 \text{ m/s}$ is considered as the allowable level of impact velocity and is utilised further for evaluating operational limiting sea states from the response surfaces (RSs) estimated for impact velocities.

[Fig. 23\(a\)-\(c\)](#) present the allowable limiting sea state envelope derived in terms of H_s, T_p combination for mating process for $\beta_{wave} = 0^\circ$, $\beta_{wave} = 30^\circ$, and $\beta_{wave} = 60^\circ$ respectively for a constant $U_w = 8 \text{ m/s}$. These envelopes are obtained by limiting the response surfaces of the impact velocities shown in [Fig. 18](#) by the allowable level of impact velocity obtained from the finite element analysis (FEA) results, i.e. ($V_{allow} = 0.76 \text{ m/s}$). Note that any region below or lying on the curve is operable in nature and is considered as safe for performing installation operation. On the contrary, any region above the curve is restricted and must not be considered for performing operation.

It can be seen from the figures that generally for an installation system with or without TMD, the limiting sea states are better for cases with increasing wind-wave misalignment conditions. This result is due to the impact velocities in the y -direction being maximum for collinear wave-wind condition and thus more critical compared to the misaligned conditions, where corresponding impact velocities for the same load cases are less. Furthermore, the effectiveness of the TMD on the operational limiting sea states is clearly visible for all the cases of β_{wave} , as the area under the curve with respect to the baseline case is substantially increased. In this manner, the application of TMD could indeed provide a substantial cost-efficient option for installation of wind turbine blade, as the limiting sea states for the task are expanded. Additionally, the effect of TMD on the operational limiting sea states is substantial for misalignment $\beta_{wave} = 60^\circ$ as shown in [Fig. 23\(c\)](#), where more than 85% of the sea states can be allowed for safe mating operation. One of the major advantages implied from [Fig. 23\(a\)-\(c\)](#) is that the application of TMD enables the mating process to be executed at higher H_s , e.g., $H_s = 3 \text{ m}$, and thus, the overall efficiency of the mating task is increased. This situation is beneficial for offshore installation contractors as the limiting condition for H_s which tends to be quite restrictive in practice is relaxed using TMD. One important point to mention here is that the limiting sea states presented in the figures only represents results for the range of load cases considered in the paper. Care must be considered while extrapolating results to higher or lower values of H_s and T_p . In principle, the analysis must be considered for all possible values of environmental load cases possible at an offshore site, however here only a range of sea states that are considered operable by experience were chosen and were listed in [Table 3](#).

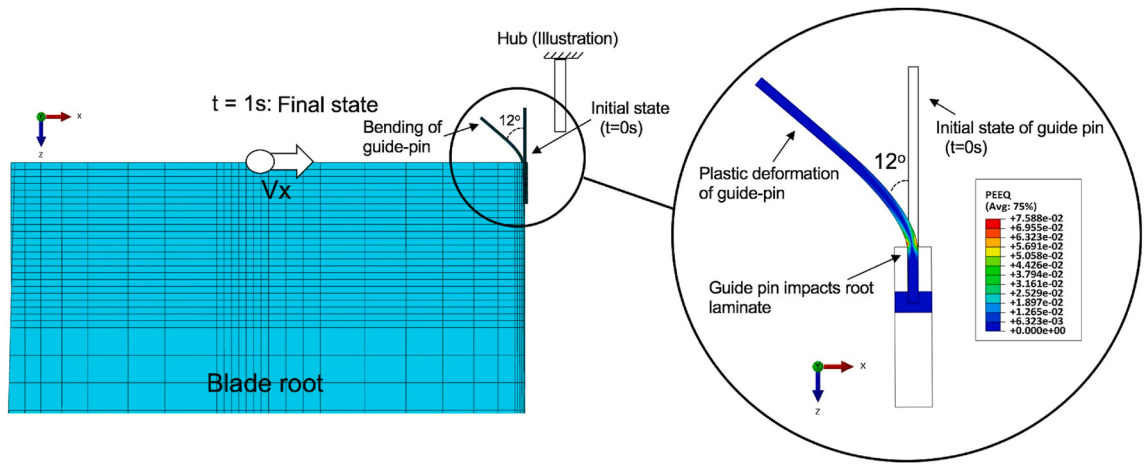


Fig. 20. Bending and plastic deformation of the guide pin ($V_x^{fem} = 0.85m/s$).

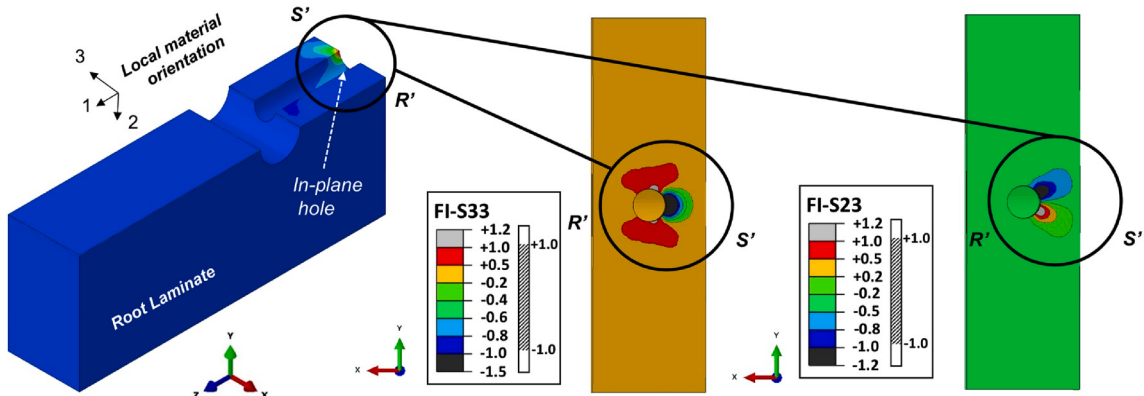


Fig. 21. Failure index with stress exposure factors at the inplane hole of the root laminate ($V_x^{fem} = 0.85m/s$).

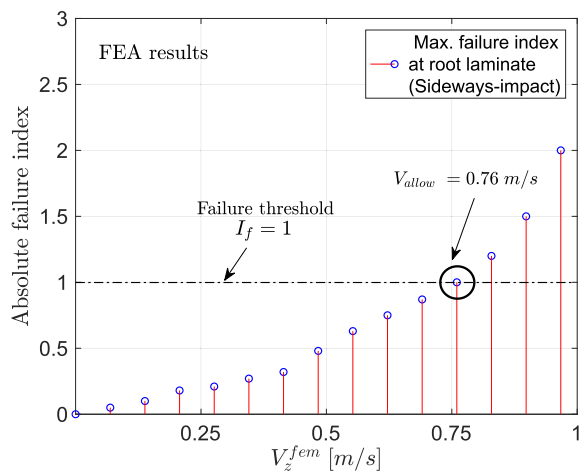


Fig. 22. Estimation of threshold velocity of impact at the blade root.

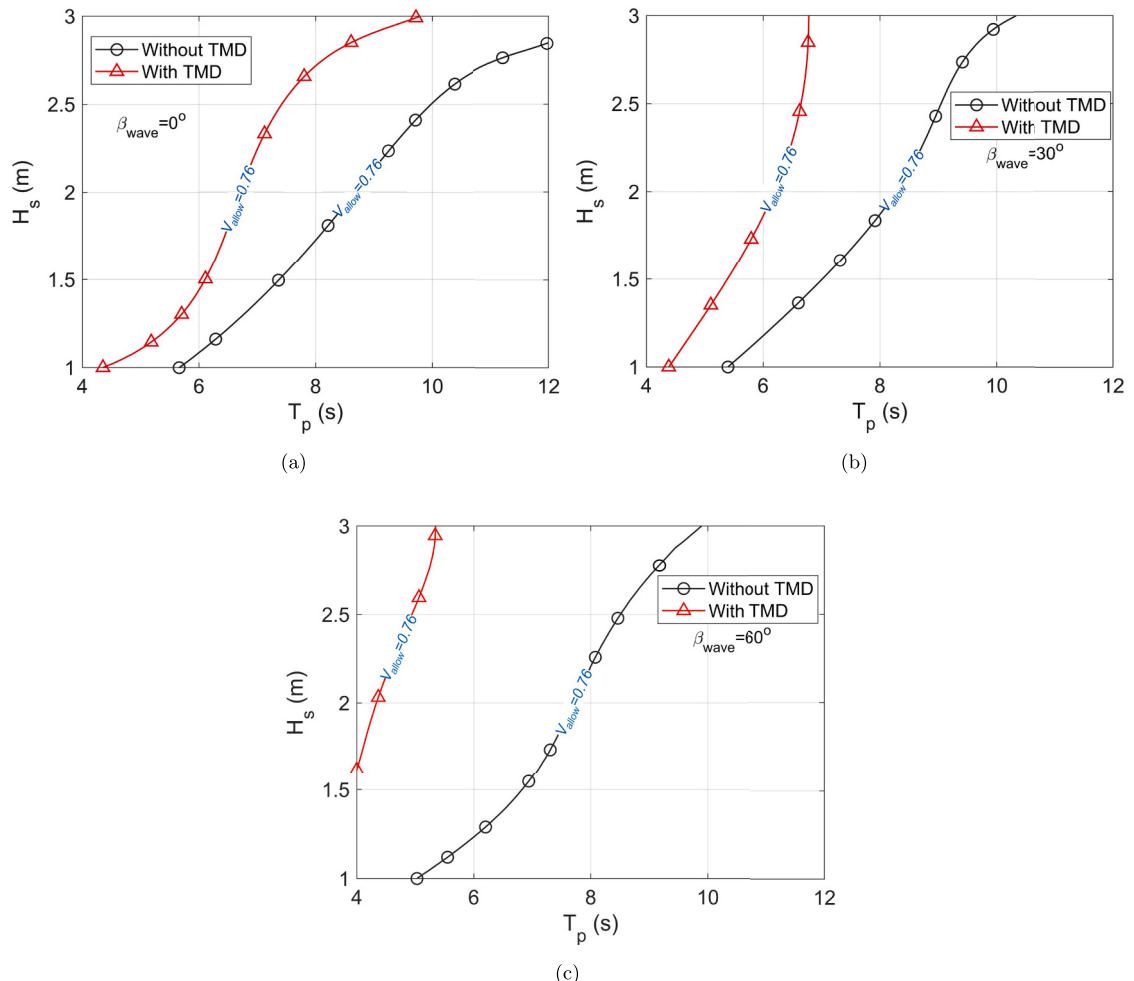


Fig. 23. Limiting sea states for blade mating task considering installation system with and without TMD (a) $\beta_{\text{wave}} = 0^\circ$ (b) $\beta_{\text{wave}} = 30^\circ$ (c) $\beta_{\text{wave}} = 60^\circ$.

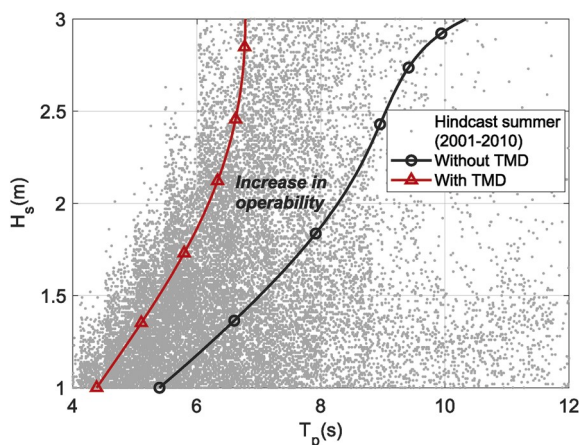


Fig. 24. Comparison of operability with and without TMD.

4.5. Brief discussion on operability

Here, we discuss briefly the potential of a TMD for increasing the operability of a mating operation between blade root and the hub. This parameter aids offshore contractors to plan the time available to execute an offshore installation activity in a safe manner. Based on the derived allowable limiting sea states, reference period for the task, and hindcast data of the site with details of sea state parameters, operability can be judged. Fig. 24 presents the hindcast data for H_s and T_p occurrences (represented in the figure by small grey dots) for the ‘North sea centre’ offshore site for 10 years of summer months (i.e., May–September). It can be clearly seen from the density of the dots that the site has a high occurrence of low T_p , which is critical for hub motions, as it is near the eigenperiod of the monopile in the first fore-aft mode. The allowable limiting sea state curves for installation system with and without TMD, for $\beta_{wave} = 30^\circ$ is also overlapped with the hindcast data (see Fig. 24) to qualitatively understand the effect on the operability. Any area below the curves is allowable and safe for the installation task. It is seen that for the case of installation system without TMD, not many data points lie below the curve, and thus, the operability is limited even though the limiting sea states without TMD look assuring. However, with the application of TMD and due to a shift in the curve of the limiting sea states, there is a significant increase in the workable window for the task given that many data points for the hindcast lie below the curve. It is to also be emphasised that although there is a modest shift in the curve from the baseline case due to the effect of TMD, it has a substantial influence on the overall the operability of the task. On a closer investigation, the operability had increased by more than 60% by considering the TMD. Hence, the application of TMD could enable increase in the weather window for the mating task, which could provide high cost efficiency during the installation task.

5. Conclusion

The present paper investigated the effect of an external passive tuned mass damper on the blade root impact during the mating process. There were two parameters focused on in this study to quantify the effectiveness of TMD. The first parameter was the impact velocity between the blade root and the hub during the mating process in the global y-direction. This could cause sideways impacts of the blade root with the hub during the mating task and is found critical in determining the structural damage at the blade root. The second parameter was the efficacy of the TMD on the response-based allowable limiting sea states to judge its effect on the operability of the mating operation.

Time domain multibody simulations of installation system characterising mating process were performed with a tuned mass damper, which was connected to the HAWC2 aeroelastic code using a force DLL formulated in Fortran. Different environmental load cases were considered, and the impact velocities developed the root and hub in the y-direction were quantified. Analytical relationships between the impact velocity and sea state parameters H_s and T_p was developed using the response surface method (RSM) and were presented for different wind-wave misalignment conditions (β_{wave}). Finite element analyses were also performed for the case in which the blade root with a guide pin suffers a sideways impact with the hub, and the threshold level of impact velocity was determined. Based on this threshold level, and for a given response surface obtained for different β_{wave} , allowable sea states for the mating operation were derived and compared between installation systems with and without the TMD. A brief discussion regarding the effect of the TMD on the operability of the mating task was also discussed. The following are the main conclusions from the study:

- (1). The tuned mass damper system was mounted onto the tower structure during installation and consisted of a single-degree-of-freedom system acting in the fore-aft direction of the monopile. The parameters of the TMD were optimised, and the damping ratio of the monopile system in the fore-aft mode increased from 1% critical to 5.6%. As a result of this increase in the damping ratio, the hub-centre motion in the y-direction was reduced substantially. The effect was substantial at T_p close to the resonance frequency of the monopile in the fore-aft mode and decreased with increased spectral wave peak period.
- (2). For collinear wind and waves conditions, the motion of the hub centre is almost exclusively in the fore-aft direction, with the TMD effect only in the y-direction. However, for wind-wave misalignment conditions considered for $\beta_{wave} = 30^\circ, 60^\circ$, it was found that the motion of the hub centre is significant both in the x- and y-directions and is correlated. Furthermore, the TMD reduces the motion of the hub in xy-plane and presents an inclined nature of attenuation.
- (3). The spectrum of impact velocity developed between root and hub showed several peaks contributed from blade motion, wave frequency and monopile motion. However, the TMD only reduces the peak contributed from the eigenfrequency of the monopile in the first fore-aft mode.
- (4). The analytical relationship between the impact velocity and sea state parameters showed that the response surface of the TMD is smaller than the baseline without the TMD. The response surface of impact velocity generally decreases with β_{wave} .
- (5). The effectiveness of the TMD in reducing the impact velocities varies with various parameters. The efficiency increases with increasing H_s but decreases with increasing misalignment between wind and wave conditions (β_{wave}) and with the wave spectral peak period diverging from the tuned frequency of the monopile system. A TMD system with optimised parameters has the capacity to reduce the impact velocities by more than 40%.
- (6). Several cases of impact velocities were considered for the finite element analysis for the case in which a single guide pin impacts the hub. It was found that the velocity of impact corresponding to 0.85 m/s lies above the threshold level, given the damage developed in the root laminate, which corresponded to a failure index greater than 1. The velocity of impact of 0.76 m/s was found to be the allowable impact velocity, which was the threshold level for damage to occur in the root laminate.

- (7). Based on the threshold level of impact velocity and for a given response surface, allowable sea states were derived in terms of H_s and T_p for installation system with and without a TMD. It was found that the TMD could substantially expand limiting sea states for the mating task and thus provide high operability and an expanded weather window, which is a cost-effective option.

6. Limitations and future work

In the current work, the application potential of a TMD device during the wind turbine blade mating process was studied. Certain simplifications and assumptions were made, especially during the numerical modelling based on which the limiting sea state for the operation was compared for systems with and without TMD. The allowable impact velocity obtained from the finite element study was based on maximum stress failure criterion, where damages were predicted on a homogenised root laminate. In principle, a highly fidelity progressive failure analysis needs to be performed at ply-level to obtain an accurate estimate, especially focusing at the point where the delamination cracks appears. This will be considered in the future work, where progressive failure finite element models will be developed and validated with experiment. Also, different guide pins with different material strength parameter is expected to give varying levels of structural strength threshold and thus a sensitivity study for a proper choice of guide-pin material needs to be understood. In addition, the purpose of the TMD system used in this study is to inhibit motion sensitivity of the monopile structure contributed from its first fore-aft mode as such conditions causes sideways impact of the guide pin during mating. As a result, a TMD is installed inside the turbine tower and is not directly exposed to effects of sea water temperature. However, for other modes of deformation of the monopile system, the position of TMD system needs to be modified and can be influenced by the sea water temperature. These effects require investigation in the future work. Further, the effect of sudden disturbances because of earthquakes is essential to be included and needs to be addressed in the future work. In such cases it might also be important to include stroke constrained conditions on the TMD [36].

Declaration of competing interest

No conflicts of interest to disclose.

Acknowledgement

This work was made possible through the SFI MOVE projects supported by the Research Council of Norway, NFR project number 237929.

References

- [1] Acero WIG. Assessment of marine operations for offshore wind turbine installation with emphasis on response-based operational limits [PhD thesis]. Trondheim: Norwegian University of Science and Technology (NTNU); 2016.
- [2] Wind Europe. The European offshore wind industry—Key trends and statistics. 2017. Technical Report.
- [3] Kuijken L. Single blade installation for large wind turbines in extreme wind conditions [Master thesis]. Technical University of Denmark; 2015.
- [4] He W, Yin Z, Sun C. Adaptive neural network control of a marine vessel with constraints using the asymmetric barrier lyapunov function. *IEEE Trans Cybern* 2016;47(7):1641–51.
- [5] Jiang Z, Gao Z, Ren Y, Li Zhengru, Lei D. A parametric study on the blade final installation process for monopile wind turbines under rough environmental conditions. *Eng Struct* 2018;172:1042–56.
- [6] Jiang Z. The impact of a passive tuned mass damper on offshore single-blade installation. *J Wind Eng Ind Aerod* 2018;176:65–77.
- [7] Verma AS, Jiang Z, Vedvik NP, Gao Z, Ren Z. Impact assessment of a wind turbine blade root during an offshore mating process. *Eng Struct* 2019;180:205–22.
- [8] Habali S, Saleh I. Local design, testing and manufacturing of small mixed airfoil wind turbine blades of glass fiber reinforced plastics: part I: design of the blade and root. *Energy Convers Manag* 2000;41(3):249–80.
- [9] Martínez V, Güemes A, Trias D, Blanco N. Numerical and experimental analysis of stresses and failure in t-bolt joints. *Compos Struct* 2011;93(10):2636–45.
- [10] Veldkamp H, Van Der Tempel J. Influence of wave modelling on the prediction of fatigue for offshore wind turbines. *Wind Energy* 2005;8(1):49–65.
- [11] Damgaard M, Ibsen LB, Andersen LV, Andersen JK. Cross-wind modal properties of offshore wind turbines identified by full scale testing. *J Wind Eng Ind Aerod* 2013;116:94–108.
- [12] Shirzadeh R, Weijtjens W, Guillaume P, Devriendt C. The dynamics of an offshore wind turbine in parked conditions: a comparison between simulations and measurements. *Wind Energy* 2015;18(10):1685–702.
- [13] Zhao Y, Cheng Z, Sandvik PC, Gao Z, Moan T. An integrated dynamic analysis method for simulating installation of a single blade for offshore wind turbines. *Ocean Eng* 2017;152:72–88.
- [14] Ren Z, Jiang Z, Skjetne R, Gao Z. Development and application of a simulator for offshore wind turbine blades installation. *Ocean Eng* 2018;166:380–95.
- [15] H. W. Nv, The boom lock, <http://www.high-wind.eu/boomlock/> (Accessed: Feb 21, 2017).
- [16] Electronic Wind Solutions. Offshore tagline system. 2015. <https://www.eltronic-ws.com/products/tagline-system/>. Accessed on 7/16/2018.
- [17] Eric Van Buren, Private communication with eric van Buren, fred. Olsen windcarrier (Accessed: April 18, 2018).
- [18] <http://www.seajacks.com/offshore-wind-solutions/>. Picture.
- [19] https://www.siemens.com/press/en/events/2012/energy/2012_09-london.php. Picture.
- [20] Spencer Jr B, Nagarajaiah S. State of the art of structural control. *J Struct Eng* 2003;129(7):845–56.
- [21] Lackner MA, Rotea MA. Passive structural control of offshore wind turbines. *Wind Energy* 2011;14(3):373–88.
- [22] http://www.xiengineering.com/design_solutions/tmd. Picture.
- [23] <https://www.esmgmbh.de>. Picture.
- [24] Soto MG, Adeli H. Tuned mass dampers. *Arch Comput Methods Eng* 2013;20(4):419–31.
- [25] Kwok K, Samali B. Performance of tuned mass dampers under wind loads. *Eng Struct* 1995;17(9):655–67.
- [26] Kaynia AM, Biggs JM, Veneziano D. Seismic effectiveness of tuned mass dampers. *J Struct Div* 1981;107(8):1465–84.
- [27] Mensah AF, Dueñas-Osorio L. Improved reliability of wind turbine towers with tuned liquid column dampers (tlcds). *Struct Saf* 2014;47:78–86.
- [28] Colwell S, Basu B. Tuned liquid column dampers in offshore wind turbines for structural control. *Eng Struct* 2009;31(2):358–68.
- [29] Hagood NW, von Flotow A. Damping of structural vibrations with piezoelectric materials and passive electrical networks. *J Sound Vib* 1991;146(2):243–68.

- [30] Schwarzenahl SM, Szwedowicz J, Neubauer M, Panning L, Wallaschek J. On blade damping technology using passive piezoelectric dampers. In: ASME turbo expo 2012: turbine technical conference and exposition. American Society of Mechanical Engineers; 2012. p. 1205–15.
- [31] Djajakesukma S, Samali B, Nguyen H. Study of a semi-active stiffness damper under various earthquake inputs. *Earthq Eng Struct Dynam* 2002;31(10):1757–76.
- [32] Lam AH-F, Liao W-H. Semi-active control of automotive suspension systems with magneto-rheological dampers. *Int J Veh Des* 2003;33(1–3):50–75.
- [33] Murtagh P, Ghosh A, Basu B, Broderick B. Passive control of wind turbine vibrations including blade/tower interaction and rotationally sampled turbulence. *Wind Energy*: Int. J Progr Appl Wind Power Convers Technol 2008;11(4):305–17.
- [34] Lackner MA, Rotea MA. Structural control of floating wind turbines. *Mechatronics* 2011;21(4):704–19.
- [35] Stewart GM, Lackner MA. The impact of passive tuned mass dampers and wind-wave misalignment on offshore wind turbine loads. *Eng Struct* 2014;73:54–61.
- [36] Hu Y, He E. Active structural control of a floating wind turbine with a stroke-limited hybrid mass damper. *J Sound Vib* 2017;410:447–72.
- [37] Si Y, Karimi HR, Gao H. Modeling and parameter analysis of the oc3-hywind floating wind turbine with a tuned mass damper in nacelle. *J Appl Math* 2013;2013: Hindawi.
- [38] He E-M, Hu Y-Q, Zhang Y. Optimization design of tuned mass damper for vibration suppression of a barge-type offshore floating wind turbine. *Proc IME M J Eng Marit Environ* 2017;231(1):302–15.
- [39] Si Y, Karimi HR, Gao H. Modelling and optimization of a passive structural control design for a spar-type floating wind turbine. *Eng Struct* 2014;69:168–82.
- [40] Yang J, He E, Hu Y. Dynamic modeling and vibration suppression for an offshore wind turbine with a tuned mass damper in floating platform. *Appl Ocean Res* 2019;83:21–9.
- [41] Xie S, Jin X, He J. Structural vibration control for the offshore floating wind turbine including drivetrain dynamics analysis. *J Renew Sustain Energy* 2019;11(2): 023304.
- [42] Zuo H, Bi K, Hao H. A state-of-the-art review on the vibration mitigation of wind turbines. *Renew Sustain Energy Rev* 2020;121:109710.
- [43] Stewart G, Lackner M. Offshore wind turbine load reduction employing optimal passive tuned mass damping systems. *IEEE Trans Contr Syst Technol* 2013;21(4):1090–104.
- [44] Lian J, Zhao Y, Lian C, Wang H, Dong X, Jiang Q, Zhou H, Jiang J. Application of an eddy current-tuned mass damper to vibration mitigation of offshore wind turbines. *Energies* 2018;11(12):3319.
- [45] Zuo H, Bi K, Hao H. Using multiple tuned mass dampers to control offshore wind turbine vibrations under multiple hazards. *Eng Struct* 2017;141:303–15.
- [46] Hussan M, Rahman MS, Sharmin F, Kim D, Do J. Multiple tuned mass damper for multi-mode vibration reduction of offshore wind turbine under seismic excitation. *Ocean Eng* 2018;160:449–60.
- [47] Kim S-Y, Lee C-H. Analysis and optimization of multiple tuned mass dampers with coulomb dry friction. *Engineering Structures*; 2019. p. 110011.
- [48] Dinh V-N, Basu B. Passive control of floating offshore wind turbine nacelle and spar vibrations by multiple tuned mass dampers. *Struct Contr Health Monit* 2015; 22(1):152–76.
- [49] Hu Y, Wang J, Chen MZ, Li Z, Sun Y. Load mitigation for a barge-type floating offshore wind turbine via inerter-based passive structural control. *Eng Struct* 2018;177:198–209.
- [50] Zhang R, Zhao Z, Dai K. Seismic response mitigation of a wind turbine tower using a tuned parallel inerter mass system. *Eng Struct* 2019;180:29–39.
- [51] Tong X, Zhao X, Zhao S. Load reduction of a monopile wind turbine tower using optimal tuned mass dampers. *Int J Contr* 2017;90(7):1283–98.
- [52] Zhao B, Gao H, Wang Z, Lu Z. Shaking table test on vibration control effects of a monopile offshore wind turbine with a tuned mass damper. *Wind Energy* 2018; 21(12):1309–28.
- [53] Sun C, Jahangiri V. Bi-directional vibration control of offshore wind turbines using a 3d pendulum tuned mass damper. *Mech Syst Signal Process* 2018;105: 338–60.
- [54] Sun C, Jahangiri V, Sun H. Performance of a 3d pendulum tuned mass damper in offshore wind turbines under multiple hazards and system variations. *Smart Struct Syst* 2019;24(1):53–65.
- [55] Jahangiri V, Sun C. Integrated bi-directional vibration control and energy harvesting of monopile offshore wind turbines. *Ocean Eng* 2019;178:260–9.
- [56] Chen J-L, Georgakis CT. Spherical tuned liquid damper for vibration control in wind turbines. *J Vib Contr* 2015;21(10):1875–85.
- [57] Ghaemmaghami A, Kianoush R, Yuan X-X. Numerical modeling of dynamic behavior of annular tuned liquid dampers for applications in wind towers. *Comput Aided Civ Infrastruct Eng* 2013;28(1):38–51.
- [58] Ha M, Cheong C. Pitch motion mitigation of spar-type floating substructure for offshore wind turbine using multilayer tuned liquid damper. *Ocean Eng* 2016; 116:157–64.
- [59] Zhang Z, Staino A, Basu B, Nielsen SR. Performance evaluation of full-scale tuned liquid dampers (tlds) for vibration control of large wind turbines using real-time hybrid testing. *Eng Struct* 2016;126:417–31.
- [60] Zhang Z, Basu B, Nielsen SR. Real-time hybrid aeroelastic simulation of wind turbines with various types of full-scale tuned liquid dampers. *Wind Energy* 2019; 22(2):239–56.
- [61] Altay O, Butenweg C, Klinkel S, Taddei F. Vibration mitigation of wind turbine towers by tuned liquid column dampers. In: Proceedings of the IX international conference on structural dynamics, Porto, Portugal, vol. 12; 2014.
- [62] Buckley T, Watson P, Cahill P, Jaksic V, Pakrashi V. Mitigating the structural vibrations of wind turbines using tuned liquid column damper considering soil-structure interaction. *Renew Energy* 2018;120:322–41.
- [63] Zhang Z, Hoeg C. Vibration control of floating offshore wind turbines using liquid column dampers. In: Journal of physics: conference series, vol. 1037. IOP Publishing; 2018, 032002.
- [64] Chen J, Liu Y, Bai X. Shaking table test and numerical analysis of offshore wind turbine tower systems controlled by tlcd. *Earthq Eng Eng Vib* 2015;14(1):55–75.
- [65] Jiang Z, Trond S, Kvialkarimrad M, Machiladies C, Shi W, Verma A. Effect of a passive tuned mass damper on offshore installation of a wind turbine nacelle. *J Marine Sci Appl* 2020. Under review.
- [66] Brøndsted P, Nijssen RP. Advances in wind turbine blade design and materials. Elsevier; 2013.
- [67] Peeters M, Santo G, Degroote J, Paepengem WV. The concept of segmented wind turbine blades: a review. *Energies* 2017;10(8):1112.
- [68] Eriksen BM. Wind and tidal turbine blade root connection [Master's thesis]. Trondheim: Norwegian University of Science and Technology (NTNU); 2011.
- [69] Larsen TJ. How 2 hawc2, the user's manual, Tech. rep.. Risø National Laboratory, Technical University of Denmark; 2009.
- [70] Larsen TJ, Hansen AM. How 2 HAWC2, the user's manual, Tech. rep.. Risø National Laboratory; 2007.
- [71] Bak C, Zahle F, Bitsche R, Kim T, Yde A, Henriksen LC, Hansen MH, Natarajan A. Description of the DTU 10 MW reference wind turbine, progress report Report-I-0092. DTU Wind Energy; 2013.
- [72] Velarde J. Design of monopile foundations to support the DTU 10 MW offshore wind turbine [Master thesis]. Trondheim: Norwegian University of Science and Technology (NTNU); 2016.
- [73] Shirzadeh R, Devriendt C, Bidakhviti MA, Guillaume P. Experimental and computational damping estimation of an offshore wind turbine on a monopile foundation. *J Wind Eng Ind Aerod* 2013;120:96–106.
- [74] Morison J, Johnson J, Schauf S, et al. The force exerted by surface waves on piles. *J Petrol Technol* 1950;2(5):149–54.
- [75] Faltinsen O. Sea loads on ships and offshore structures. Cambridge university press; 1993.
- [76] Mann J. The spatial structure of neutral atmospheric surface-layer turbulence. *J Fluid Mech* 1994;273:141–68.
- [77] Hoerner SF. Fluid-dynamic drag: practical information on aerodynamic drag and hydrodynamic resistance. NJ, USA: Hoerner Fluid Dynamics Midland Park; 1965.
- [78] Irfanoglu A. CE573 structural dynamics". Purdue University College of Engineering; 2016.
- [79] La Cava W, Lackner M. Theory manual for the tuned mass damper module in fast v8, Tech. rep.. Department of Mechanical and Industrial Engineering, University of Massachusetts Amherst; 2015.
- [80] H. Hibbit, B. Karlsson, P. Sorensen, Abaqus analysis users manual version 2016.
- [81] Tanlak N, Sonmez F, Talay E. Detailed and simplified models of bolted joints under impact loading. *J Strain Anal Eng Des* 2011;46(3):213–25.

- [82] Camanho PP. Failure criteria for fibre-reinforced polymer composites, Secção de Mecânica Aplicada, Departamento de Engenharia Mecânica e Gestão Industrial. Faculdade de Engenharia da Universidade do Porto; 2002.
- [83] Haselbach PU, Branner K. Initiation of trailing edge failure in full-scale wind turbine blade test. *Eng Fract Mech* 2016;162:136–54.
- [84] Hu Y, Yang B, Nie SD, Da GX. Performance of high strength structural bolts in tension: effects of tolerance classes. In: International conference on performance-based and life-cycle structural engineering. School of Civil Engineering, The University of Queensland; 2015. p. 776–81.
- [85] Montgomery DC. Design and analysis of experiments. John Wiley & Sons; 2017.
- [86] Verma AS, Gao Z, Jiang Z, Ren Z, Vedvik NP. Structural safety assessment of marine operations from a long-term perspective: a case study of offshore wind turbine blade installation. In: ASME 2019 38th international conference on ocean, offshore and arctic engineering. American Society of Mechanical Engineers Digital Collection; 2019.